Struct Multidisc Optim (2013) 48:685–710
DOI 10.1007/s00158-013-0935-4

REVIEW ARTICLE

A critical comparative assessment of differential equation-driven methods for structural topology optimization

Arun L. Gain · Glaucio H. Paulino

Received: 21 October 2012 / Revised: 8 March 2013 / Accepted: 29 March 2013 / Published online: 3 July 2013

Abstract In recent years, differential equation-driven methods have emerged as an alternate approach for structural topology optimization. In such methods, the design is evolved using special differential equations. Implicit level-set methods are one such set of approaches in which the design domain is represented in terms of implicit functions and generally (but not necessarily) use the Hamilton-Jacobi equation as the evolution equation. Another set of approaches are referred to as phase-field methods; which generally use a reaction-diffusion equation, such as the Allen-Cahn equation, for topology evolution. In this work, we exhaustively analyze four level-set methods and one phase-field method, which are representative of the literature. In order to evaluate performance, all the methods are implemented in MATLAB and studied using two-dimensional compliance minimization problems.

Keywords Differential equation-driven methods · Level-set method · Hamilton-Jacobi equation · Phase-field method · Allen-Cahn equation · Compliance minimization

1 Introduction

Topology optimization refers to the optimum distribution of a material in a given design space, under certain specified boundary conditions, so as to optimize prescribed performance objectives. Some of the early topology optimization approaches include homogenization methods (Bendsøe and Kikuchi 1988; Suzuki and Kikuchi 1991; Allaire and Kohn 1993), and its variants, such as the Solid Isotropic Material with Penalization (SIMP) method (Bendsøe 1989; Rozvany et al. 1992; Bendsøe and Sigmund 1999). Recently, some new approaches for topology optimization have come forth in which the design is driven by differential equations. One such approach uses the level-set method (Osher and Sethian 1988; Sethian 1999b; Osher and Fedkiw 2003), c.f. Fig. 1, in which the fronts and free boundaries evolve using the Hamilton-Jacobi equation. The level-set methods utilize the implicit level-set functions to represent the geometry; which allows for determination of structural boundaries. The level-set method is a computationally tractable and versatile method, which has been adapted in a variety of fields such as fluid mechanics (Sussman et al. 1994; Chang et al. 1996; Zhou and Li 2008; Duan et al. 2008; Challis and Guest 2009), optics (Kao et al. 2005; He et al. 2007), image processing, solids modeling, and computer animation (Ye et al. 2002; Tsai and Osher 2003; Osher and Fedkiw 2003). In addition, the level-set method has also been used to solve thermal problems (Ha and Cho 2005; Zhuang et al. 2007; Xia and Wang 2008; Kim et al. 2009; Iga et al. 2009; Maute et al. 2011; Yamada et al. 2011).

Shape and topology optimization using level-sets have been explored by many researchers (Sethian and Wiegmann 2000; Osher and Santosa 2001; Allaire et al. 2002; Wang et al. 2003; Allaire et al. 2004). Wang et al. (2003) presented a structural topology optimization method for bi-material systems and studied the compliance minimization problem for linear elastic materials. Wang and Wang (2004) extended Wang et al. (2003) method to multi-material systems. During the same time, Allaire et al. (2002, 2004) proposed a structural optimization technique combining the classical shape derivative and the level-set method. They solved

A. L. Gain · G. H. Paulino (✉)
Department of Civil and Environmental Engineering, University of Illinois at Urbana-Champaign, 205 N. Mathews Ave., Urbana, IL 61801, USA
e-mail: paulino@uiuc.edu

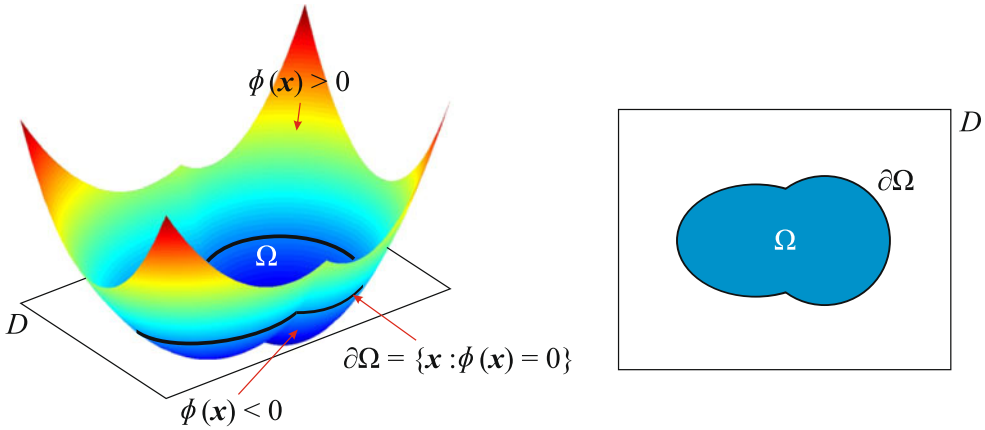

Fig. 1 Representation of design domain D using implicit function (level-sets). This is an alternative approach to explicit parameterization of the geometry

the compliance minimization, compliant mechanism design, and design dependent load problems for linear elastic systems and also investigated nonlinear elasticity problems. Both Wang et al. (2003) and Allaire et al. (2004) used an upwind scheme (Sethian 1999b) for the discrete solution of the Hamilton-Jacobi equation. Later, Allaire and Jouve extended their level-set method for eigenvalue, multiple load (Allaire and Jouve 2005) and minimum stress design problems (Allaire and Jouve 2008). Also, Yamada et al. (2010) and Yamasaki et al. (2010) solved the free vibration eigenvalue topology problem using the level-set method. Other researchers (Wei and Wang 2006; Luo et al. 2008a, b; Challis and Guest 2009) have also used shape sensitivities for the evolution of design using the level-set methods.

There have been some attempts to develop level-set methods which do not involve solving the Hamilton-Jacobi equation for the evolution of shapes. For example, Belytschko et al. (2003) proposed a topology optimization method where the weak form of the equilibrium equation is expressed as a Heaviside step function of the level-set function. The Heaviside function is subsequently regularized to enable evaluation of sensitivities of the objective functions and constraints. Van Dijk (Van Dijk et al. 2009; Van Dijk 2012) developed a method where the design domain is implicitly represented by a level-set function and the design is evolved using a steepest-descent type update scheme which utilizes the discrete sensitivities of the objective function. Non-Hamilton-Jacobi based level-set methods can also be seen in the fluid topology optimization literature. Cunha (2004) presented an Eulerian-type parametric level-set based shape optimization method where the design domain is expressed in terms of level-sets and the design variables are defined at the mesh vertices. They used it to obtain shapes which reproduce a particular velocity field for incompressible, viscous fluid using Navier-Stokes and Stokes flow models. Pingen et al. (2010) examined a parametric level-set method for fluid topology optimization using a hydrodynamic Lattice Boltzmann method. Kreissl et al. (2011) find the optimal layout of fluidic devices employing an explicit level-set method along with a Lattice Boltzmann solver. No-slip boundary conditions are enforced along the solid-fluid interface using second-order accurate interpolation schemes. Kreissl and Maute (2012) use an approach similar to Kreissl et al. (2011) and model the flow field by the incompressible Navier-Stokes equations discretized by the extended finite element method (XFEM). Also, they enforce a no-slip condition along the solid-fluid interface by applying the stabilized Lagrange multiplier method.

Hamilton-Jacobi based level-set methods generally have a tendency to become too steep near the boundaries (hence have high spatial gradients) or too flat during the course of evolution, thus affecting the accuracy and rate of convergence of the level-set method, see Fig. 2. Without any control over the gradients near the boundaries, the evolution algorithm tends to become unstable (indicated by sharp rise in the level-set values), leading to an inaccurate estimation of the boundary normal.

One option to control the gradients is to periodically reinitialize the level-set function; for example, to a signed-distance function, to maintain the numerical accuracy. In one reinitialization approach, the zero level-set function isocontour; which represents the shape boundary, is approximated using the same shape functions as in FEM and then the distances from the discretized isocontour are computed (Chopp 1993; Yamasaki et al. 2010). Another popular approach is to solve a specifically tailored partial differential equation (Sussman et al. 1994; Allaire et al. 2004). Alternatively, Sethian (1999a, b) proposed a reinitialization scheme, known as Fast Marching Method (FMM), which allows one to solve the boundary value problem, without any iteration, using an optimal ordering of the grid points.

The works of Sethian and Wiegmann (2000), Wang et al. (2003) and Allaire et al. (2004) illustrate that level-set methods allow for drastic change in topology during evolution, but can have final configurations that are very sensitive to the chosen initial configuration. This problem can be attributed to the fact that there are no inherent hole

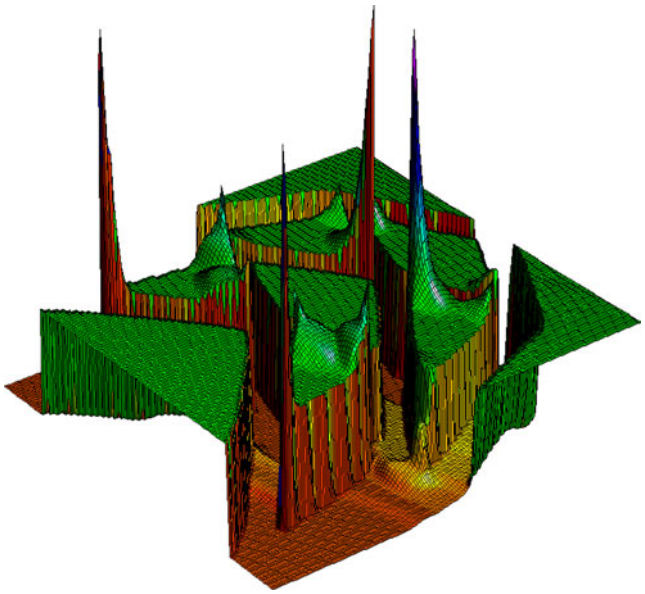

Fig. 2 Level-set function without any slope control near the design boundaries

nucleation mechanisms in the level-set based topology optimization methods for two-dimensional problems. Pre-existing holes can only merge or cancel. Several attempts have been made to alleviate this issue. One set of popular approaches is the use of topological derivatives. Topological derivative approaches can be further sub-categorized into two strategies. In the first strategy, holes are nucleated by removing material from the locations where the topological derivative takes the least value (Allaire et al. 2005; Wang 2005). A second strategy modifies the Hamilton-Jacobi equation to include topological sensitivity information (Burger et al. 2004; Amstutz and Andrä 2006; He et al. 2007; Challis 2010). Amstutz and Andrä (2006) only use topological derivatives and no shape derivatives in their evolution equation. Another hole nucleation approach is based on radial basis functions (Wang and Wang 2006; Wang et al. 2007a, b; Ho et al. 2013). This approach does not make use of topological derivative information; instead the Hamilton-Jacobi equation is reduced to a set of ordinary differential equations using multi-quadratic splines and solved using Euler's method. The elimination of reinitialization and adoption of smoothed naturally extended velocities aids the creation of new holes. Use of radial basis functions helps maintain the smoothness of the level-set function. Other researchers have also used radial basis functions to parameterize the level-set function (De Ruiter and Van Keulen 2004; Wei and Wang 2006; Luo et al. 2007; Kreissl et al. 2011). In case of three-dimensional optimization, Allaire et al. (2004) have shown that the traditional level-set approach using the Hamilton-Jacobi equation with shape derivatives is able to nucleate new holes in the domain due to the pinching of thin walls. Others researchers (e.g. Challis et al. 2008, 2012) have arrived at similar conclusions for three-dimensional optimization with the level-set method. Recently, Van Dijk et al. (2013) published a review article which provides a detailed overview of the different level-set methods for structural topology optimization.

Phase-field based methods are another category of approaches rapidly gaining popularity. Essentially, the phase-field method is a diffuse interface model where boundaries between phases are not sharp, but considered to have a finite thickness, hence providing a smooth transition for the physical quantities between the phases. It has been used in materials science to study the phase transition phenomenon. Cahn and Hillard (1958), and Allen and Cahn (1979) used the theory of phase transition to study the liquid phases with variable densities. Phase-field methods have been applied in a wide variety of fields such as fracture mechanics (Aranson et al. 2000), visual reconstruction (March 1992), and crystal growth simulations (Kobayashi 1993). Bourdin and Chambolle (2003) used the phase-field method to study compliance minimization problems subjected to design dependent loads such as pressure and gravity. Wang and Zhou (2004a) used the van der Waals-Cahn-Hillard phase transition theory to propose a phase-field method for topology optimization of a design domain consisting bi-phase systems. Later, Wang and Zhou (2004b) extended the method to tri-phase systems. In addition, Burger and Stainko (2006) proposed a phase-field method based relaxation scheme for structural topology optimization problems with local stress constraints. Takezawa et al. (2010) utilized the Allen-Cahn equation (Allen and Cahn 1979), a time dependent reaction-diffusion equation, for the evolution of topologies in structural optimization problems. The uniqueness of their approach was the utilization of the objective function sensitivity to construct the double well potential function.

The goal of the current work is to study some of the prominent, and characteristically different, level-set and phase-field methods which are representative of the literature. Our efforts focus on critically understanding the following five methods: the AJT level-set method (Allaire et al. 2004), the DLK level-set method (Van Dijk et al. 2009), the WW level-set method (Wang and Wang 2006), Challis' level-set method (Challis 2010) and the TNK phase-field method (Takezawa et al. 2010).[1] *We acknowledge that the cited authors may have substantially improved their methods after the aforementioned papers were published. We would like to clarify that our goal is not to address the latest contributions of each author, but to investigate what has been reported in the five specific papers cited above, namely* Allaire et al. (2004), Van Dijk (2009),

[1] The acronyms, AJT, DLK, WW and TNK are used to abbreviate the last name of the authors in each corresponding paper.

Wang and Wang (2006), Challis (2010), and Takezawa et al. (2010). Although, the level-set and phase-field methods have been used to study a wide variety of problems subjected to different constraints, we will focus on *two-dimensional compliance minimization problems* only. It should be noted that the methods covered in this work are representative and not exhaustive of the differential equation driven methods for topology optimization. We hope this work will be a guide for future additional developments in the field of topology optimization.

We would like to remark that the literature tends to focus on solving topology optimization problems on Cartesian meshes. In this work, we also use uniform grids to discretize rectangular design domains. When dealing with complicated domains, accurate representation of design domains and boundary conditions requires additional effort. An efficient way to deal with complicated domains is to use polygonal elements (c.f. Gain and Paulino 2012; Talischi et al. 2010).

The remainder of the paper is organized as follows. Section 2 discusses the formulation of the topology optimization problem. Section 3 briefly reviews the differential equation-driven methods analyzed in this work. Section 4 discusses the results of our analysis of these methods, using several numerical examples. Finally, Section 5 provides some concluding remarks.

2 Topology optimization framework

In the current work, we focus on compliance minimization problems for linearized elastic systems. Compliance, which is the work done by applied loads, is given by:

$$J(\phi) = \int_D \boldsymbol{f} \cdot \boldsymbol{u}\, d\boldsymbol{x} + \int_{\partial D_{\mathrm{N}}} \boldsymbol{g} \cdot \boldsymbol{u}\, ds = \int_D \boldsymbol{C}^*(\phi)\boldsymbol{\varepsilon}(\boldsymbol{u}) \cdot \boldsymbol{\varepsilon}(\boldsymbol{u})\, d\boldsymbol{x} \tag{1}$$

where $\boldsymbol{f}$ is the body force, $\boldsymbol{g}$ represents the surface loads and $\boldsymbol{C}^*$ is the effective elasticity tensor which depends on the design function ϕ (discussed in detail in the subsequent section), and the dot denotes the inner product. Also, $\boldsymbol{u}$ represents the displacement field, which is obtained by solving the state equations below:

$$\begin{aligned} -\boldsymbol{\nabla} \cdot \left(\boldsymbol{C}^*(\phi)\boldsymbol{\varepsilon}(\boldsymbol{u})\right) &= \boldsymbol{f} \quad && \text{in } D, \\ \boldsymbol{u} &= \boldsymbol{0} && \text{on } \partial D_{\mathrm{D}}, \\ \left(\boldsymbol{C}^*(\phi)\boldsymbol{\varepsilon}(\boldsymbol{u})\right) \cdot \boldsymbol{n} &= \boldsymbol{g} && \text{on } \partial D_{\mathrm{N}}, \\ \left(\boldsymbol{C}^*(\phi)\boldsymbol{\varepsilon}(\boldsymbol{u})\right) \cdot \boldsymbol{n} &= \boldsymbol{0} && \text{on } \partial D_0. \end{aligned} \tag{2}$$

where $\boldsymbol{\varepsilon}$ is the linearized strain, $\boldsymbol{\varepsilon}(\boldsymbol{u}) = {}^1/_2(\boldsymbol{\nabla u} + \boldsymbol{\nabla u}^T)$, and D represents the working domain; which contains all the admissible shapes Ω, i.e., $\Omega \subset D$ and its boundary ∂D consists of three disjoint components, $\partial D = \partial D_{\mathrm{D}} \cup \partial D_0 \cup \partial D_{\mathrm{N}}$. Here ∂D_{D}, ∂D_0, and ∂D_{N} correspond to Dirichlet boundary conditions, homogeneous Neumann boundary conditions, and non-homogeneous Neumann boundary conditions with $\boldsymbol{g} \neq \boldsymbol{0}$, respectively. The body force is assumed to be zero, $\boldsymbol{f} = \boldsymbol{0}$, for all the examples in the current study. Also, the design Ω, with boundary $\partial\Omega = \Gamma_N \cup \Gamma_D$, is constrained to satisfy $\Gamma_{\mathrm{N}} = \partial D_{\mathrm{N}} \cup \Gamma_0$ and $\Gamma_{\mathrm{D}} \subset \partial D_{\mathrm{D}}$. Here, Γ_D, Γ_N, and Γ_0 correspond to the boundary of Ω with Dirichlet, Neumann, and homogeneous Neumann boundary conditions, respectively (c.f. Fig. 3).

The compliance minimization problem entails finding the stiffest configuration under the applied loads and boundary conditions. For nontrivial solutions, we impose a volume constraint $P(\phi) = \left(\int_D \rho(\phi)\, d\boldsymbol{x} - V_{max}\right)$ on the problem (1) using the Lagrange multiplier method to obtain the following unconstrained optimization problem:

$$\inf_{\phi} \bar{J}(\phi) = J(\phi) + \lambda P(\phi) \tag{3}$$

where λ, $\rho(\phi)$ and V_{max} are the positive Lagrange multiplier, density function and prescribed volume fraction, respectively. In discrete form (3) can be rewritten as:

$$\inf_{\phi} \bar{J}(\phi) = \boldsymbol{F}^T\boldsymbol{U} + \lambda\left(\boldsymbol{V}^T\boldsymbol{\rho}(\phi) - V_{max}\right) \tag{4}$$

where $\boldsymbol{F}$ is the discretized global force vector, $\boldsymbol{U}$ is the global nodal displacement vector, $\boldsymbol{V}$ is an array of the fractional areas of elements, $\boldsymbol{V} = [A_1, A_2, ..., A_n]^T / \sum_i A_i$, the A_i's are element areas and $\boldsymbol{\rho}(\phi)$ is the element density array. In the case of level-set methods, the design function, ϕ, is defined as:

$$\begin{cases} \phi = 0 & \boldsymbol{x} \in \partial\Omega \cap D, \\ \phi < 0 & \boldsymbol{x} \in \Omega, \\ \phi > 0 & \boldsymbol{x} \in (D \setminus (\Omega \cup \partial\Omega)). \end{cases} \tag{5}$$

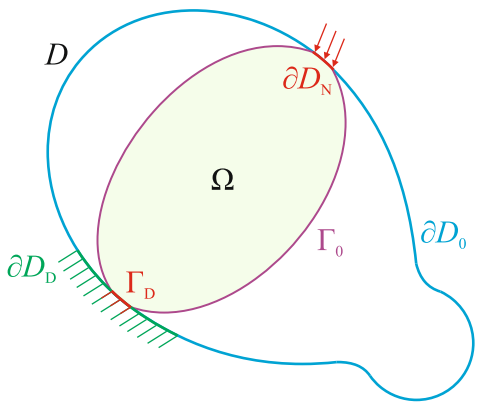

Fig. 3 Illustration of the working domain. The working domain D consists of all admissible designs, Ω. Its boundary ∂D consists of ∂D_{D} (Dirichlet boundary), ∂D_{N} (non-homogeneous Neumann boundary) and ∂D_0 (homogeneous Neumann boundary). The design Ω, with boundary $\partial\Omega = \Gamma_N \cup \Gamma_D$, is constrained to satisfy $\Gamma_{\mathrm{N}} = \partial D_{\mathrm{N}} \cup \Gamma_0$ and $\Gamma_{\mathrm{D}} \subset \partial D_{\mathrm{D}}$. Boundaries Γ_D, Γ_N, and Γ_0 correspond to Dirichlet, Neumann, and homogeneous Neumann boundary conditions on $\partial\Omega$, respectively

The phase-field method starts with the boundary conditions specified in Fig. 3. At any time during the optimization process, the phase-field domain can be illustrated by Fig. 4. The working domain, D, is considered to be composed of two phases (Ω_0, Ω_1) and the interfacial boundary between the phases, ξ, which is called the diffuse interface (Fig. 4). The diffuse interface acts as the transition zone between the two phases. The working domain D contains all admissible shapes Ω, i.e., $\Omega \subset D$. Here $\Omega \subset (\Omega_1 \cup \xi)$. Accordingly, the design function, ϕ, for the phase-field method is defined as:

$$\begin{cases} \phi = 1 & \boldsymbol{x} \in \Omega_1, \\ 0 < \phi < 1 & \boldsymbol{x} \in \xi, \quad \text{Diffuse interface} \\ \phi = 0 & \boldsymbol{x} \in \Omega_0. \end{cases} \tag{6}$$

For uniformity of notation, we represent the design variable as ϕ for both the level-set and phase-field methods. However, for the phase-field method, the design function, ϕ, is the same as the density function, ρ.

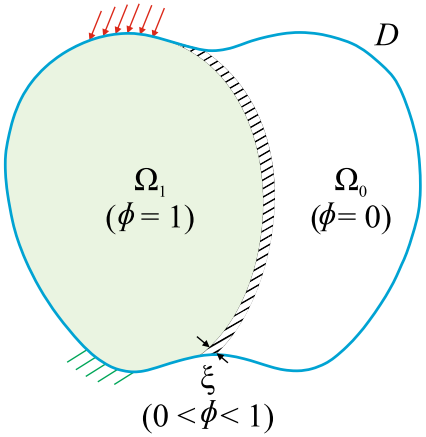

Fig. 4 Phase-field working domain D. Domains Ω_1, Ω_0 and ξ represent solid phase, void phase and diffuse interface, respectively. Here, ϕ represents the design function

3 A brief review of differential equation-based methods

Two general categories of differential equation-driven approaches for topology optimization can be found in the literature - level-set methods and phase-field methods. We specifically selected four representative level-set approaches and one representative phase-field approach to review in this work. We first present a brief summary of the five methods.

3.1 AJT level-set method (Allaire et al. 2004)[2]

In the level-set method proposed by Allaire et al. (2004), the design front propagation is governed by the Hamilton-Jacobi equation and the advection velocity is derived from a shape sensitivity analysis. The solid phase, $\phi < 0$, is assumed to be filled with material of elasticity tensor $\boldsymbol{C}$. In order to avoid singularities in the global stiffness matrix, the void region, $\phi > 0$, is filled with a weak phase with elasticity tensor $k_{min}\boldsymbol{C}$. Here, k_{min} is chosen as 10^{-3}. This is called the Ersatz material approach. Thus, the effective elasticity tensor $\boldsymbol{C}^*$ for the entire design domain D is defined as:

$$\boldsymbol{C}^*(\phi) = \rho_e(\phi)\boldsymbol{C} \quad \text{with} \quad \rho_e(\phi) = \begin{cases} 1 & \phi < 0, \\ k_{min} & \phi > 0. \end{cases} \tag{7}$$

Here, density ρ_e is taken as piecewise constant for each element. The procedure to calculate element densities for the elements which are cut by the zero level-set function is not clearly described in Allaire et al. (2004). One possible approach is provided by Allaire et al. (2012). In this approach, first the rectangular element is split into four triangles and the central node is assigned the average of the level-set function values at the rectangular vertices. Then, linear interpolation is used to obtain densities corresponding to each triangle. The element density is the average of the densities of the constituent triangles.

The topology is evolved over fictitious time using the Hamilton-Jacobi equation:

$$\frac{\partial \phi}{\partial t} + v\,|\boldsymbol{\nabla}\phi| = 0, \qquad \frac{\partial \phi}{\partial \boldsymbol{n}} = 0 \text{ on } \partial \mathrm{D} \tag{8}$$

where $\boldsymbol{n}$ is the normal vector and the advection velocity, v, is obtained from the shape sensitivity analysis. For objective (3), v is given as:

$$v = \boldsymbol{\varepsilon}(\boldsymbol{u})^T \boldsymbol{C}^* \boldsymbol{\varepsilon}(\boldsymbol{u}) - \lambda \tag{9}$$

In our implementation, design function, ϕ, is nodal based. Hence, the velocities need to be calculated at the nodes as well. First, (9) is integrated over each finite element to obtain elemental velocities. Velocities at the nodes are obtained by taking the average of the elemental velocities surrounding each node. We use a second order upwind scheme (Sethian 1999b) to solve (8).

$$\phi_{i,j}^{n+1} = \phi_{i,j}^{n} - \Delta t \left(\max\left(v_{i,j}, 0\right) \boldsymbol{\nabla}^{+} + \min(v_{i,j}, 0) \boldsymbol{\nabla}^{-} \right) \tag{10}$$

[2] All the discussions about the AJT method (Allaire et al. 2004) in Sections 4 and 5 are based on our own implementation.

Here, $\phi^n_{i,j}$, $v_{i,j}$ are values of ϕ, v for the nth iteration at the node located at $\boldsymbol{x}_{i,j}$. The parameters $\boldsymbol{\nabla}^+$ and $\boldsymbol{\nabla}^-$ in (10) are given by:

$$\begin{aligned}\boldsymbol{\nabla}^+ &= \Big[\max(A_1,0)^2+\min(A_2,0)^2 \\ &\quad +\max(A_3,0)^2+\min(A_4,0)^2\Big]^{1/2} \\ \boldsymbol{\nabla}^- &= \Big[\max(A_2,0)^2+\min(A_1,0)^2 \\ &\quad +\max(A_4,0)^2+\min(A_3,0)^2\Big]^{1/2}\end{aligned} \tag{11}$$

where the terms A_1, A_2, A_3, A_4 are:

$$\begin{aligned}A_1 &= D^{-x}_{i,j}+\frac{\Delta x}{2}m\left(D^{-x-x}_{i,j},D^{+x-x}_{i,j}\right),\\ A_2 &= D^{+x}_{i,j}-\frac{\Delta x}{2}m\left(D^{+x+x}_{i,j},D^{+x-x}_{i,j}\right),\\ A_3 &= D^{-y}_{i,j}+\frac{\Delta y}{2}m\left(D^{-y-y}_{i,j},D^{+y-y}_{i,j}\right),\\ A_4 &= D^{+y}_{i,j}-\frac{\Delta y}{2}m\left(D^{+y+y}_{i,j},D^{+y-y}_{i,j}\right).\end{aligned} \tag{12}$$

The function m and derivatives $D^{+x+x}_{i,j}$, $D^{+x-x}_{i,j}$, D^{+x} and D^{-x} are defined as:

$$m(x,y)=\begin{cases}\begin{cases}x & \text{if } |x|\le|y|\\ y & \text{if } |x|>|y|\end{cases} & \text{for } xy\ge 0,\\ 0 & \text{for } xy<0.\end{cases} \tag{13}$$

$$\begin{aligned}D^{+x+x} &= \frac{\phi^n_{i+2,j}-2\phi^n_{i+1,j}+\phi^n_{i,j}}{(\Delta x)^2},\\ D^{+x-x} &= \frac{\phi^n_{i+1,j}-2\phi^n_{i,j}+\phi^n_{i-1,j}}{(\Delta x)^2},\end{aligned} \tag{14}$$

$$D^{+x}=\frac{\phi^n_{i+1,j}-\phi^n_{i,j}}{\Delta x},\qquad D^{-x}=\frac{\phi^n_{i,j}-\phi^n_{i-1,j}}{\Delta x}. \tag{15}$$

Other derivatives, $D^{-x-x}_{i,j}$, $D^{+y+y}_{i,j}$, $D^{+y-y}_{i,j}$, $D^{-y-y}_{i,j}$, D^{+y} and D^{-y}, can be calculated in a similar way. Also, Δx and Δy are the distances between the nodes in the x and y direction, respectively. Over the course of evolution, the level-set function may become too steep or too flat which may result in an inaccurate approximation of the normal, $\boldsymbol{n}$. For numerical accuracy, the level-set function needs to be reinitialized/smoothed periodically. Reinitialization to a signed distance function is one option; which can be achieved by solving the equation:

$$\frac{\partial\phi}{\partial t}+sign(\phi_0)\left(|\boldsymbol{\nabla}\phi|-1\right)=0,\qquad \frac{\partial\phi}{\partial\boldsymbol{n}}=0 \text{ on } \partial\mathrm{D} \tag{16}$$
$$\text{with}\quad \phi(x,t=0)=\phi_0(x).$$

At steady state, the above equation reduces to $|\boldsymbol{\nabla}\phi|=1$, the solution of which is a signed distance function. A second order upwind scheme, discussed previously, is used to solve the reinitialization (16).

3.2 DLK level-set method (Van Dijk et al. 2009)[3]

Traditionally, level-set methods use shape derivatives to estimate the advection velocity for the Hamilton-Jacobi equation. Van Dijk et al. (2009) proposed a modified version of level-set method, which uses discrete sensitivity of the objective function in a steepest-descent type evolution scheme. Their work was motivated by the argument that the use of shape sensitivities to derive the velocity field may cause inconsistencies in the discretization of the velocity field and governing equations, which may lead to poor performance. They also dealt with multiple constraints, which is not very common in the literature of differential equation-driven methods for topology optimization. The authors use an adjoint approach to calculate the discrete sensitivities, modifying the objective function (4) by adding the zero function $\boldsymbol{Q}^T\boldsymbol{R}\left(\boldsymbol{\rho}(\phi),\boldsymbol{U}\right)$ as follows:

$$\inf_{\phi}\bar{J}(\phi)=\boldsymbol{F}^T\boldsymbol{U}+\lambda\left(\boldsymbol{V}^T\boldsymbol{\rho}(\phi)-V_{max}\right)+\boldsymbol{Q}^T\boldsymbol{R}\left(\boldsymbol{\rho}(\phi),\boldsymbol{U}\right) \tag{17}$$

where $\boldsymbol{Q}$ is a Lagrange multiplier vector and $\boldsymbol{R}\left(\boldsymbol{\rho}(\phi),\boldsymbol{U}\right)$ is the residual obtained from the finite element discretization of the equilibrium equation. Apart from the volume constraint, the authors also impose displacement constraint on the optimization problem. As mentioned earlier, for simplicity, we will only investigate the compliance minimization problem with volume constraint. The sensitivity of the objective function (4) is calculated by differentiating (17) as follows:

$$\frac{\partial\bar{J}}{\partial\boldsymbol{\phi}}=\frac{\partial\bar{J}}{\partial\boldsymbol{\rho}}\frac{\partial\boldsymbol{\rho}}{\partial\boldsymbol{\phi}}=\left(\boldsymbol{Q}^T\frac{\partial\boldsymbol{R}}{\partial\boldsymbol{\rho}}+\lambda\boldsymbol{V}^T\right)\frac{\partial\boldsymbol{\rho}}{\partial\boldsymbol{\phi}} \tag{18}$$

where $\boldsymbol{Q}$ is computed by solving the adjoint system:

$$\frac{\partial\bar{J}}{\partial\boldsymbol{U}}=\boldsymbol{F}^T+\boldsymbol{Q}^T\frac{\partial\boldsymbol{R}}{\partial\boldsymbol{U}}=\boldsymbol{0} \tag{19}$$

In the level-set literature, it is often not clear how the level-set function is mapped to the density domain in the design interface region. The authors (Van Dijk et al. 2009), however, present a clear mapping scheme using an approximate Heaviside function as shown below:

$$\rho_e(\phi)=\frac{\int_{\Omega_e}H(\phi)d\Omega}{\int_{\Omega_e}d\Omega} \tag{20}$$

[3]The discussions on the DLK method (Van Dijk et al. 2009) in Sections 4 and 5 are based on our implementation.

where Ω_e represents the element domain and $H(\phi)$ is an approximate Heaviside function given by (c.f. Fig. 5):

$$H(\phi) = \begin{cases} 1 & \phi < -h, \\ \frac{1}{4}(1-\epsilon)\left(\left(\frac{\phi}{h}\right)^3 - 3\left(\frac{\phi}{h}\right) - 2\right) + 1 & -h \le \phi \le h, \\ \epsilon & \phi > h. \end{cases} \tag{21}$$

Here, $h = d/10$, where d is the length of the diagonal of the finite element. Thus, $\partial \boldsymbol{\rho}/\partial \boldsymbol{\phi}$, needed to evaluate the objective function sensitivity, can be calculated as:

$$\frac{\partial \rho_e}{\partial \phi_i} = \frac{\int_{\Omega_e} \delta(\phi) N_i \, d\Omega}{\int_{\Omega_e} d\Omega} \tag{22}$$

where $\delta(\phi)$ is the derivative (Dirac delta function) of the approximate Heaviside function (21):

$$\delta(\phi) = \begin{cases} 0 & \phi < -h, \\ \frac{1}{4}(1-\epsilon)\left(\frac{3\phi^2}{h^3} - \frac{3}{h}\right) & -h \le \phi \le h, \\ 0 & \phi > h. \end{cases} \tag{23}$$

The integral in the numerator of (20) and (22) is approximated by sampling ϕ at 10×10 points over each finite element. In the literature, other approximate Heaviside based mapping schemes can be found which utilize polynomial functions (Wang et al. 2003; Lui et al. 2005; Kawamoto et al. 2011; Van Dijk 2012) and trigonometric functions (Belytschko et al. 2003; Haber 2004; Luo et al. 2008a; Pingen et al. 2010). Finally, the level-set is evolved according to the following direct update scheme:

$$\boldsymbol{\phi}^{n+1} = \boldsymbol{\phi}^n - t \frac{\partial \bar{J}/\partial \boldsymbol{\phi}}{\left\| \partial \bar{J}/\partial \boldsymbol{\phi} \right\|} \tag{24}$$

where $\boldsymbol{\phi}^n$ and t represent the design function array at the nth iteration and scaling constant, respectively. As mentioned before, the authors' update scheme (24) is different from the typical advection equation updates (8) used for the level-set methods. The DLK approach requires very frequent reinitialization to achieve convergence and this is because the direct update (24) does not preserve the magnitude of the gradient of the level-set function. Reinitialization is performed using (16).

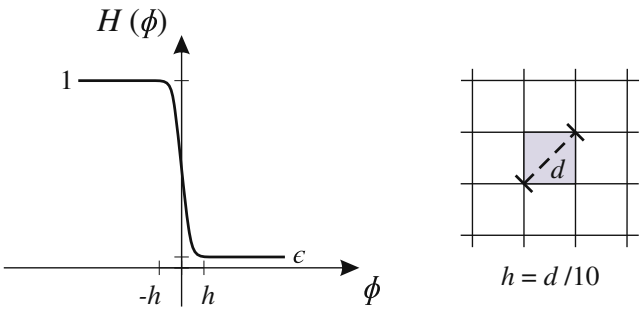

Fig. 5 Approximate Heaviside function to evaluate element densities in the elements cut by the zero level-set, $\phi = 0$

3.3 WW level-set method (Wang and Wang 2006)[4]

We next look at the radial basis function based level-set method proposed by Wang and Wang (2006). Similar approaches can be seen in Wang et al. (2007a, b). Radial basis functions are radially symmetric functions centered at a specific point. Wang and Wang (2006) used a particular form of radial basis functions, known as multi-quadric splines, and method of lines to transform the Hamilton-Jacobi partial differential equation into a system of ordinary differential equations. The authors claim that their method does not require reinitialization (which is expensive) and is insensitive to initial designs. The general form of a radial basis function, centered around $\boldsymbol{x}_i$, can be written as $N_i(\boldsymbol{x}) = N(\|\boldsymbol{x} - \boldsymbol{x}_i\|)$. The multi-quadratic splines used in their work can be expressed as:

$$N_i(\boldsymbol{x}) = \sqrt{(\boldsymbol{x} - \boldsymbol{x}_i)^2 + c_i^2} \tag{25}$$

where c_i is assumed to be a constant shape parameter which affects the flatness of the splines. The design function, $\phi(\boldsymbol{x})$, can be written in terms of multi-quadratic splines with m nodes or knots as:

$$\phi(\boldsymbol{x}) = \sum_{i=1}^{m} \alpha_i N_i(\boldsymbol{x}) + p(\boldsymbol{x}) \tag{26}$$

where α_i is the weight of the radial basis function at the ith knot and $p(\boldsymbol{x}) = p_0 + p_1 x + p_2 y$ is a first degree polynomial to account for the linear and constant portions of the function. Using the orthogonality conditions $\left(\sum_i^m \alpha_i = 0, \ \sum_i^m \alpha_i x_i = 0, \ \sum_i^m \alpha_i y_i = 0\right)$ and the given function values at m knots $(\phi(\boldsymbol{x}_i) = f_i, \ i = 1, 2, ..., m)$, we get a system of $m + 3$ linear equations to solve for $m + 3$ unknown coefficients. In matrix notation, the above equations can be written as:

$$\boldsymbol{H}\boldsymbol{\alpha} = \boldsymbol{f} \tag{27}$$

where

$$\boldsymbol{H} = \begin{bmatrix} \boldsymbol{P}_N & \boldsymbol{P}_X \\ \boldsymbol{P}_X^T & \boldsymbol{0} \end{bmatrix}, \quad \boldsymbol{P}_N = \begin{bmatrix} N_1(\boldsymbol{x}_1) & \cdots & N_m(\boldsymbol{x}_1) \\ \vdots & \ddots & \vdots \\ N_1(\boldsymbol{x}_m) & \cdots & N_m(\boldsymbol{x}_m) \end{bmatrix}, \quad \boldsymbol{P}_X = \begin{bmatrix} 1 & x_1 & y_1 \\ \vdots & \vdots & \vdots \\ 1 & x_m & y_m \end{bmatrix} \tag{28}$$

[4]The discussions pertaining to the WW method (Wang and Wang 2006) in Sections 4 and 5 are based on our implementation.

$$\boldsymbol{\alpha} = [\alpha_1 \ \cdots \ \alpha_m \ p_0 \ p_1 \ p_2]^T, \qquad \boldsymbol{f} = [f_1 \ \cdots \ f_m \ 0 \ 0 \ 0]^T \tag{29}$$

Thus, (26) can be written as, $\phi(\boldsymbol{x}) = \boldsymbol{N}^T(\boldsymbol{x})\,\boldsymbol{\alpha}$, where $\boldsymbol{N}^T(\boldsymbol{x}) = \left[N_1(\boldsymbol{x}) \ \cdots \ N_m(\boldsymbol{x}) \ 1 \ x \ y\right]^T$. The Hamilton-Jacobi equation, used to update the level-set function, is both space and pseudo-time dependent. In the WW approach (Wang and Wang 2006), space and time are assumed to be separable and the time dependency is lumped into the coefficients $\boldsymbol{\alpha}$. So we have

$$\phi(\boldsymbol{x}, t) = \boldsymbol{N}^T(\boldsymbol{x})\boldsymbol{\alpha}(t) \tag{30}$$

Using (30), the Hamilton-Jacobi equation (c.f. (8)) can be simplified into following ODE:

$$\boldsymbol{H}\frac{d\boldsymbol{\alpha}}{dt} + \boldsymbol{B}(\boldsymbol{\alpha}) = 0 \tag{31}$$

where

$$\boldsymbol{B}(\boldsymbol{\alpha}) = \begin{bmatrix} v(\boldsymbol{x}_1)|\boldsymbol{\nabla}\boldsymbol{N}^T(\boldsymbol{x}_1)\boldsymbol{\alpha}| \\ \vdots \\ v(\boldsymbol{x}_m)|\boldsymbol{\nabla}\boldsymbol{N}^T(\boldsymbol{x}_m)\boldsymbol{\alpha}| \\ 0 \\ 0 \\ 0 \end{bmatrix} \tag{32}$$

The authors chose Euler's method to solve the ODE (31). So, coefficients $\boldsymbol{\alpha}$ are updated as:

$$\boldsymbol{\alpha}\left(t^{n+1}\right) = \boldsymbol{\alpha}(t^n) - \Delta t\,\boldsymbol{H}^{-1}\boldsymbol{B}\left(\boldsymbol{\alpha}\left(t^n\right)\right) \tag{33}$$

Over the course of the evolution, the level-set function may become either too steep at the design interface or too flat. Typically, in the level-set method literature, in order to maintain its regularity, the level-set function is reinitialized periodically to a signed distance function. Wang and Wang (2006) argued that due to infinite smoothness of the radial basis functions, accuracy of the normal vector can be maintained and thus operations such as reinitialization are not required. In our implementation of the WW method, we too have not used any reinitialization. We will discuss this issue in detail in Section 4. They use the shape derivatives to define the advection velocity at the design front; which is extended to the entire domain using the assumption that the strain is zero in the void region, $\boldsymbol{\varepsilon} = \boldsymbol{0}$. To aid in the smooth progress of the front, they introduce the following scheme for the advection velocity:

$$v(\boldsymbol{x}) = \begin{cases} \boldsymbol{\varepsilon}(\boldsymbol{u})^T\boldsymbol{C}^*\boldsymbol{\varepsilon}(\boldsymbol{u}) - \lambda & \phi(\boldsymbol{x}) < -h, \\ \widehat{v}(\boldsymbol{x}) & -h \le \phi(\boldsymbol{x}) \le h, \\ -\lambda & \phi(\boldsymbol{x}) > h. \end{cases} \tag{34}$$

Here, $\widehat{v}(\boldsymbol{x})$ is smoothed advection velocity around the zero level-set (design boundary) which can be written as:

$$\widehat{v}(\boldsymbol{x}) = \frac{\sum_{\boldsymbol{p}\in\boldsymbol{Z}} W(\|\boldsymbol{p}-\boldsymbol{x}\|)\, v(\boldsymbol{x})}{\sum_{\boldsymbol{p}\in\boldsymbol{Z}} W(\|\boldsymbol{p}-\boldsymbol{x}\|)} \tag{35}$$

where

$$W(\|\boldsymbol{p}-\boldsymbol{x}\|) = r_{min} - \|\boldsymbol{p}-\boldsymbol{x}\| \tag{36}$$

Also, the parameter $h = 1$, and $\boldsymbol{Z}$ is the neighborhood of $\boldsymbol{x}$, such that $-h \le \phi(\boldsymbol{x}) \le h$, inside the filter window of radius r_{min}. The effect of the smoothed velocity field is discussed in Section 4.6. We use (20) to map the level-set function to the density domain. Note that, in the WW approach (Wang and Wang 2006), no mapping scheme is specified.

3.4 Challis' level-set method (Challis 2010)[5]

Recently, Challis (2010) published an educational article on the level-set method. In her work, Challis utilized Burger et al. (2004) approach of modifying the traditional Hamilton-Jacobi (c.f. (8)) to include topological derivatives to generate holes and applied it to topology optimization problems. The modified Hamilton-Jacobi equation is given as:

$$\frac{\partial\phi}{\partial t} + v\,|\boldsymbol{\nabla}\phi| = -\omega g \tag{37}$$

where $g(\boldsymbol{x})$ is a scalar field that is based on the topological sensitivities of the objective function. And ω is a positive parameter which determines the influence of $g(\boldsymbol{x})$. The level-set function value is evaluated at the center of each element and is considered constant within each element. In Challis' approach, the design does not have any intermediate densities. The level-set is mapped to the density field as follows:

$$\rho_e = \begin{cases} 1 & \text{if } \phi_e < 0, \\ 0 & \text{if } \phi_e \ge 0. \end{cases} \tag{38}$$

Here, ρ_e and ϕ_e represent the element density and the level-set function value at the center of the element, respectively. We would like to point out that in Challis' approach (c.f. Challis 2010) the objective function (39) is used, which we have modified to (4) to maintain uniformity amongst the methods investigated in this work. The corresponding normal velocity, v, which is calculated using the shape sensitivities, is also updated to (9).

$$\inf_{\phi} \bar{J}(\phi) = \boldsymbol{F}^T\boldsymbol{U} + \lambda\left(\boldsymbol{V}^T\boldsymbol{\rho}(\phi) - V_{max}\right) + \tfrac{1}{2\Lambda}\left(\boldsymbol{V}^T\boldsymbol{\rho}(\phi) - V_{max}\right)^2 \tag{39}$$

[5]The discussions in Sections 4 and 5 on Challis' method are based on the code provided in Challis (2010) with few modifications, to maintain uniformity amongst methods investigated here, which are pointed out in this section.

Subsequently, the forcing term, g, evaluated using topological derivatives of the objective function (4), follows as:

$$g = \begin{cases} \frac{\pi(\lambda+2\mu)}{2\mu(\lambda+\mu)} \left(4\mu\boldsymbol{\varepsilon}(\boldsymbol{u})^T \boldsymbol{C}^*\boldsymbol{\varepsilon}(\boldsymbol{u}) \right. \\ \qquad \left. +(\lambda-\mu)\boldsymbol{u}^T\left(\boldsymbol{k}_{\mathrm{Tr}}\right)\boldsymbol{u}\right) - \pi\lambda^n & \text{if } \phi < 0, \\ 0 & \text{if } \phi \geq 0. \end{cases} \tag{40}$$

The term $\boldsymbol{u}^T\left(\boldsymbol{k}_{\mathrm{Tr}}\right)\boldsymbol{u}$ is the finite element approximation of $\mathrm{tr}(\boldsymbol{C}^*\boldsymbol{\varepsilon}(\boldsymbol{u}))\mathrm{tr}(\boldsymbol{\varepsilon}(\boldsymbol{u}))$ (Challis 2010). After substituting v and g back into the modified Hamilton-Jacobi equation (c.f. (37)), it is solved using the upwind finite difference scheme. Frequent reinitialization of the level-set function to a signed distance function is performed using MATLAB's `bwdist` function. For further details, readers are referred to Challis' paper (2010). We also modified the global stiffness matrix assembly in Challis' code to make it more efficient by using the sparse matrix assembly function available in MATLAB.

3.5 TNK phase-field method (Takezawa et al. 2010)[6]

In the current work, apart from the level-set methods discussed earlier, we also look at the recently proposed phase-field method for structural topology optimization (Takezawa et al. 2010). In the phase-field method, the solid phase, Ω_1, is filled with material having elasticity tensor $\boldsymbol{C}$ and the region, Ω_0, mimics a void with elasticity tensor $k_{min}\boldsymbol{C}$. Here, k_{min} is chosen to be 10^{-3}. The effective elasticity tensor $\boldsymbol{C}^*$ for the entire design domains (c.f. Fig. 4) can be written as:

$$\boldsymbol{C}^*(\phi) = \begin{cases} \boldsymbol{C} & \boldsymbol{x} \in \Omega_1, \\ k(\phi)\boldsymbol{C} & \boldsymbol{x} \in \xi, \\ k_{min}\boldsymbol{C} & \boldsymbol{x} \in \Omega_0. \end{cases} \tag{41}$$

where $k_{min} \leq k(\phi) \leq 1$, $k(\phi) = \phi^p$, $p = 3$. The scheme is similar to the SIMP method. The evolution of the phases is governed by the Allen-Cahn equation (a reaction-diffusion equation):

$$\frac{\partial\phi}{\partial t} = \kappa\nabla^2\phi - f'(\phi), \qquad \frac{\partial\phi}{\partial \boldsymbol{n}} = 0 \text{ on } \partial\mathrm{D} \tag{42}$$

where κ is the diffusion coefficient and $f(\phi)$ is a double well potential function. If $f(\phi)$ is chosen to satisfy the conditions $f(0) = 0$, $f(1) = \eta\frac{\bar{J}'(\phi_t)}{\|\bar{J}'(\phi_t)\|}$, and $f'(0) = f'(1) = 0$, then the optimization proceeds in the direction which minimizes the design objective. Here, η is a scaling constant, chosen as 10. One such $f(\phi)$ is given by:

$$f(\phi) = \frac{1}{4}\phi^2(1-\phi)^2 + \eta\frac{\bar{J}'(\phi_t)}{\|\bar{J}'(\phi_t)\|}\left(6\phi^5 - 15\phi^4 + 10\phi^3\right) \tag{43}$$

[6] All the discussions related to the TNK method (Takezawa et al. 2010) are based on our implementation.

where $\bar{J}'(\phi_t)$ represents the sensitivity of objective function $\bar{J}$ with respect to ϕ at time t. One way to solve the Allen-Cahn equation is by using the finite difference scheme. Since an explicit finite difference scheme forces the function ϕ to diverge when $\phi \notin [0, 1]$, a semi-implicit scheme is used to discretize the reaction term. Thus, the scheme to update ϕ can be written as:

$$\phi_{i,j}^{n+1} = \begin{cases} \frac{\phi_{i,j}^n + \Delta t(P_1+P_2)\kappa}{1-\left(1-\phi_{i,j}^n\right)r\left(\phi_{i,j}^n\right)\Delta t} & \text{for } r\left(\phi_{i,j}^n\right) \leq 0, \\ \frac{\phi_{i,j}^n\left(1+r\left(\phi_{i,j}^n\right)\Delta t\right)+\Delta t(P_1+P_2)\kappa}{1+\phi_{i,j}^n r\left(\phi_{i,j}^n\right)\Delta t} & \text{for } r\left(\phi_{i,j}^n\right) > 0. \end{cases} \tag{44}$$

where

$$r\left(\phi_{i,j}^n\right) = \phi_{i,j}^n - \frac{1}{2} - 30\eta\frac{\bar{J}'(\phi_{t1})}{\|\bar{J}'(\phi_{t1})\|}\phi_{i,j}^n\left(1-\phi_{i,j}^n\right)$$
$$P_1 = \frac{\phi_{i-1,j}^n - 2\phi_{i,j}^n + \phi_{i+1,j}^n}{(\Delta x)^2},\ P_2 = \frac{\phi_{i,j-1}^n - 2\phi_{i,j}^n + \phi_{i,j+1}^n}{(\Delta y)^2} \tag{45}$$

The time step Δt satisfies Courant-Friedrichs-Lewy (CFL) condition.

4 Comparison among methods

Now, we discuss the results of our implementation of all the above mentioned methods. First the performance of the methods is evaluated for the two-dimensional compliance minimization test problems, followed by detailed discussions on the merits and limitations of each method. We start by looking at the implementation details of our computer codes below. It should be noted that for Challis' approach we used the code provided in her paper with a slight modification in her global stiffness matrix assembly, objective function, shape sensitivities and topological sensitivities evaluation (details are provided in Section 3.4).

4.1 Implementation details

All the methods have been implemented in MATLAB and have a similar structure. The optimization algorithm consists of the following steps (c.f Fig. 6):

1. Initialize the design function based on the initial guess and set the value of various algorithm parameters.
2. Perform the following steps until convergence:
   (a) Compute the state variable $\boldsymbol{u}$ by solving the state equation (c.f. (2)).

(b) Calculate sensitivity of the objective function for the DLK level-set method and the TNK phase-field method. In the case of the AJT, WW and Challis' level-set methods, calculate the shape derivatives.
(c) Update the topology using the respective evolution equations.

3. The level-set function needs to be reinitialized from time to time to maintain the signed distance characteristic. For this purpose, (16) is made use of for the AJT and DLK methods. For Challis' method, MATLAB's `bwdist` function is used. No reinitialization is performed for the WW level-set method and the TNK phase-field method.
4. Map the current level-set function into the density domain. Phase-field function, ϕ, is taken to be the same as the density function, ρ.

4.2 Test problem - cantilever beam

We compare the performance of the methods first using the cantilever beam compliance minimization problem; which is a common benchmark problem in the literature. A Young's modulus of E = 1, and Poisson's ratio of $\nu = 0.3$, are used for all of the examples in this work and consistent units are employed. The design domain is rectangular with dimensions 2×1 and discretized using 120×60 Q4 elements. The cantilever beam is fixed on the left side and a unit vertical load is applied at the midpoint of the right side, as shown in Fig. 7. The volume fraction, V_{max}, is fixed at 0.45 by updating the Lagrange multiplier, λ, using a scheme similar to Allaire and Pantz (2006) and Takezawa et al. (2010). Optimization terminates when either the change in element densities is less than 0.1 % or the change in the objective function is less than 0.01 %. The densities are uniform inside each element. The time step, Δt, satisfies the CFL condition for the AJT, WW, Challis' level-set methods and the TNK phase-field method.

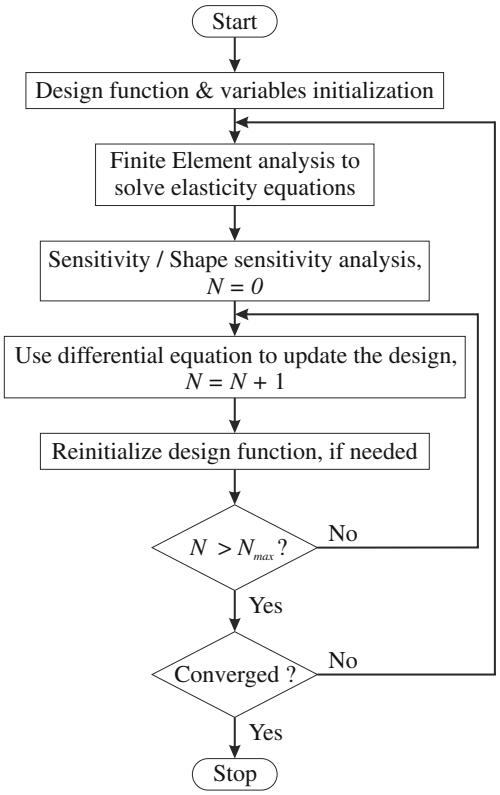

Fig. 6 Flow chart for the differential equation-driven topology optimization. Here, N_{max} represents user defined maximum number of design updates for each finite element analysis

4.2.1 Model parameters

For the AJT method, the level-set function is updated 20 times, using a second order upwind scheme for the Hamilton-Jacobi equation (c.f. (10)), for each elasticity analysis (2). The level-set function is reinitialized after every 5 update steps of the Hamilton-Jacobi equation, by conducting five explicit time steps of the second order upwind scheme of (16). In our DLK level-set method implementation, the scaling parameter is chosen as $t = h_x$, where h_x is the length of one side of the finite element. Parameter t is divided into small update steps of $t_i = h_x/4$. After every update step of t_i, using (24), the level-set is reinitialized by conducting five explicit time steps of the second order upwind scheme of (16). For the WW method implementation, the shape parameter, c, is chosen as 10^{-4}, $r_{min} = 1.2$ and $\delta = 1$. We take 2 explicit time steps of the set of ODEs obtained from the Hamilton-Jacobi equation using Euler's method (33) for each elastic finite element analysis (2). In Challis' code, the parameters `stepLength`, `numReinit` and `topWeight` (c.f. Challis 2010) are chosen as 2, 4, and 2, respectively, and the design is updated using (37). The phase-field diffusion coefficient, κ, is taken as 2×10^{-5}. We perform 20 update step evolution equation for the phase-field function, by utilizing its semi-implicit finite difference approximate (44), for every solution of state equation (c.f. (2)).

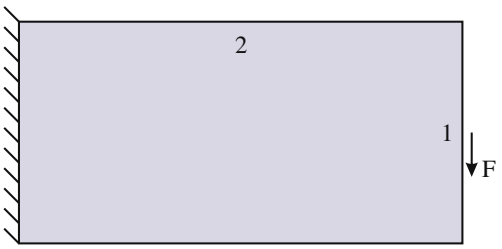

Fig. 7 Problem description of cantilever beam

4.2.2 Results

The converged topologies for the cantilever beam problem, with starting topology Fig. 8a, are shown in Fig. 8 and the summary of the results is given in Table 1. Converged configurations from the AJT level-set method (Fig. 8b), the DLK level-set method (Fig. 8c) and the TNK phase-field method (Fig. 8f) are almost identical. The DLK method produces the lowest compliance of 65.2, and all other compliances are in the range 65 to 74.

One of the drawbacks of the standard differential equation-driven methods is that new holes cannot nucleate within a structure because there is no built-in hole nucleation mechanism. However, the WW approach (Wang and Wang 2006) and Challis' approach (Challis 2010) do claim to generate holes. Hole nucleation capability may alleviate the dependence on the initial guess which we shall examine next.

4.2.3 Influence of initial guess

Typically, in differential equation driven methods, the optimal design is mesh dependent, i.e. it depends on the resolution of the design parameterization. If the design parameterization allows smaller details, the optimal design will be topologically more complex and finer members will be formed. To obtain mesh independent results, some type of length scale needs to be enforced (similar to density-based topology optimization methods; Bendsøe and Sigmund 2003). None of the five methods studied in this work enforce any length scale control. Thus, the optimal designs will have topological complexity dependent on the initial guess, unless some form of hole nucleation mechanism is introduced. This can be easily tested by evaluating the performance of the five methods for a different initial configuration. For all the methods, the design parameters are kept the same as before. The results are shown in Fig. 9.

In spite of the inclusion of hole nucleation capabilities, we observe that the WW and Challis' methods do not alleviate the dependence on the initial guess. The converged topology from Challis' approach (Fig. 9e) is still similar to other methods which can not generate holes. Although the final configuration obtained from the WW approach (Fig. 9d) is topologically more complex than the others (has more holes than the initial starting configuration), it is still not the same as the result obtained in the last problem (Fig. 8d). Further discussion on hole nucleation capabilities and other features of the WW and Challis' methods will follow in subsequent sections.

4.3 Test problem - bridge with holes

Next, we explore the problem of a bridge with holes. The design domain is rectangular in shape, discretized using 120×60 Q4 elements and is simply supported, as shown in Fig. 10. Two fixed holes are introduced into the design domain and taken care of during optimization using passive elements (Bendsøe and Sigmund 2003). All other parameters are kept the same as in the previous cantilever beam problem.

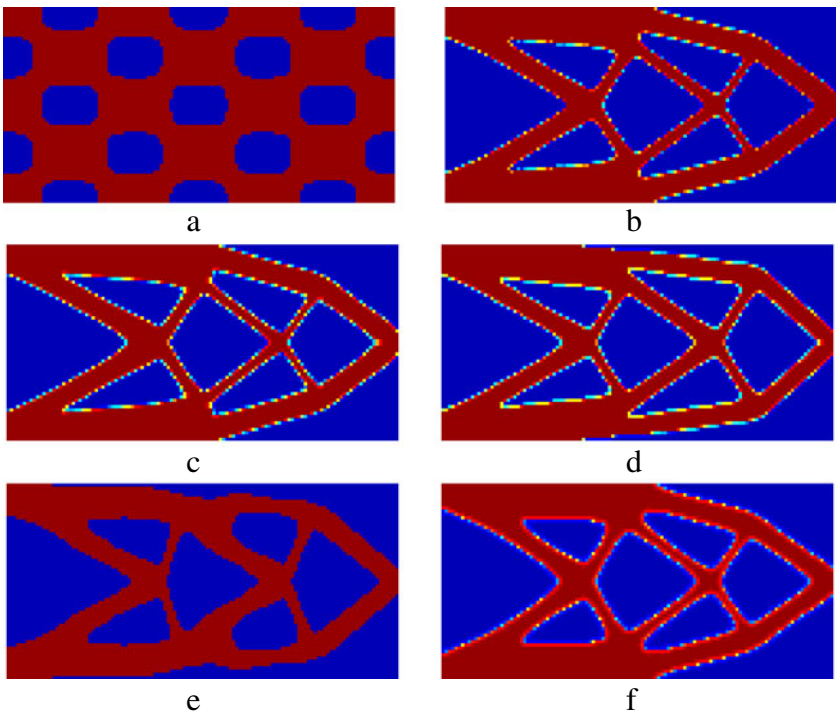

Fig. 8 Converged topologies for cantilever beam problem on a domain discretized using 120×60 mesh. **a** Initial configuration. **b** AJT level-set method. **c** DLK level-set method. **d** WW level-set method. **e** Challis' level-set code. **f** TNK phase-field method

Table 1 Summary of results shown in Fig. 8 for the cantilever beam problem. Volume fraction, $V_{max} = 0.45$, is imposed on the optimization problem

Method	Acronym	Update equation	Figure	Compliance (J)	Converged volume fraction
Allaire et al. (2004)	AJT	(10)	8b	65.9	0.45
Van Dijk et al. (2009)	DLK	(24)	8c	65.2	0.45
Wang and Wang (2006)	WW	(33)	8d	66.8	0.45
Challis (2010)	–	(37)	8e	73.8	0.45
Takezawa et al. (2010)	TNK	(44)	8f	71.6	0.45

Figure 11a is chosen as the starting topology. The converged topologies are shown in Fig. 11. Converged configurations from Challis' level-set method (Fig. 11e) and the TNK phase-field method (Fig. 11f) are visually similar, with the same number of members and similar member orientations. The AJT level-set method topology (Fig. 11b) also has the same number of members as the TNK method but with a different orientation of the middle two members. The results of the DLK method (Fig. 11c) and the WW level-set method (Fig. 11d) are clearly different from the others. In the DLK method, there are traces of intermediate densities right next to the fixed circular holes which is undesirable. The DLK method produces the least compliance of 18.5, and compliances for the other methods are fairly close to each other (in the range 18 to 22).

In the following sections, we examine each method individually.

4.4 Further discussion on the AJT level-set method

The ability to handle the merging/cancellation of holes makes the AJT level-set method suitable for topology optimization problems. As mentioned before, in the AJT method, the lack of length scale control, and an inherent hole nucleation mechanism, results in designs with topological complexity dependent on the initial guess. For such a method, it is important that the results should at least be invariant to mesh refinement when the optimization starts from a similar topology i.e. starting from a similar initial topology, the method should produce designs of similar topological complexity for different mesh discretizations. We test the invariance of the AJT method with respect to mesh refinement using the cantilever beam problem (Fig. 7) for the initialization shown in Fig. 8. The Lagrangian multiplier is kept constant at 25. The resulting converged

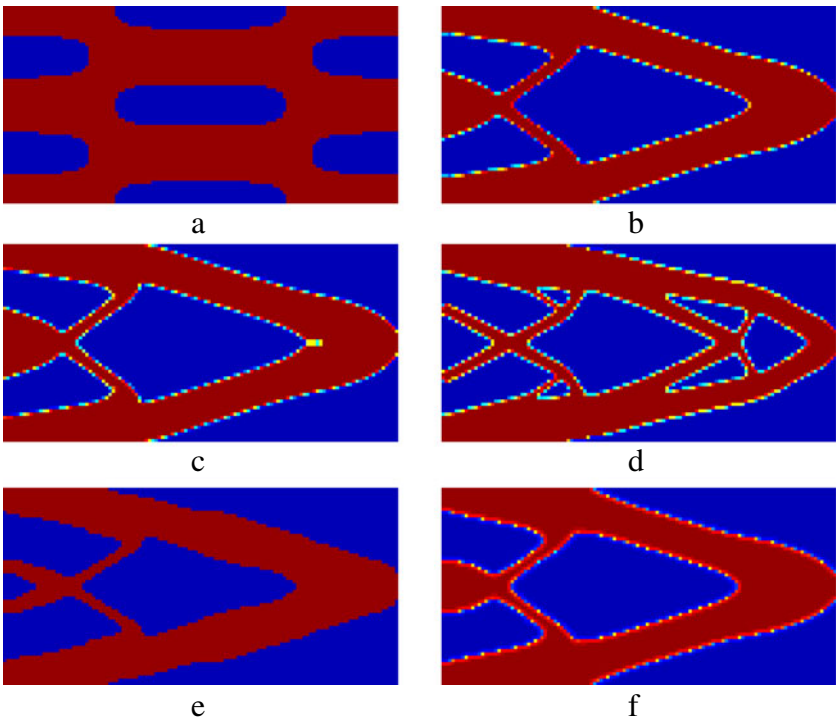

Fig. 9 Another initial configuration mesh for cantilever beam problem. **a** Initial topology. **b** AJT ($J = 76.2$). **c** DLK ($J = 75.6$). **d** WW ($J = 72.3$). **e** Challis' ($J = 80.7$). **f** TNK ($J = 80.4$)

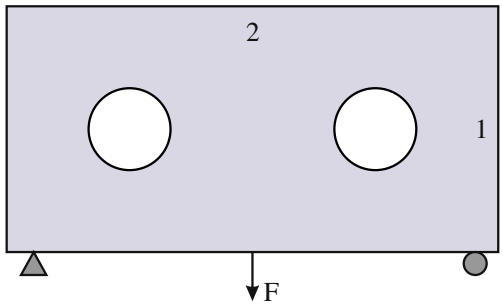

Fig. 10 Problem description of bridge with holes

designs, shown in Fig. 12, confirm that the current method is invariant to mesh refinement for similar starting topology. The compliance for the different mesh discretizations are also similar (65.8, 65.9, 66.0 and 66.2 for 80×40, 100×50, 160×80 and 200×100 mesh discretizations, respectively).

In their approach, Allaire et al. update the level-set 20 times using the Hamilton-Jacobi equation (c.f. (8)) for every solution of the state equation. Although the scheme is justified, since one explicit update step (8) is much cheaper than the solution of state (2), estimating the appropriate number of update steps per state equation solution is a vital and difficult task. A high number of steps results in an inaccurate design and a small number of steps results in a slow rate of convergence. A physically meaningful, perhaps adaptive, scheme needs to be devised to estimate the optimum number of update steps of the Hamilton-Jacobi equation (c.f. (8)) to achieve a balance between faster convergence and accurate results. It should be noted that Allaire et al. reduce the number of update steps during the course of optimization if the objective function $\bar{J}$ is not decreasing, but the exact implementation details are not provided. Similar arguments can be made for the appropriate frequency of reinitialization and the number of explicit time steps of (16) that need to be performed to maintain the signed distance nature of the level-set function. If the reinitialization (16) is solved fully until the level-set function does not change anymore, or if the reinitialization is performed very frequently, then the algorithm converges slowly. On the contrary, if insufficient reinitialization is performed, then the algorithm tends to become unstable, leading to an inaccurate estimation of the boundary normal, and ultimately converging to suboptimal topologies.

Since there are no inherent hole nucleation mechanisms in this method, the converged topology is dependent on the initial chosen topology. Allaire et al. (2005) proposed a remedy to this problem using the topological gradient method or bubble method (Eschenauer and Schumacher 1994; Sokolowski and Zochowski 1999; Céa et al. 2000; Garreau et al. 2001). In their method, the authors (Allaire et al. 2005) use the topological gradient, at a predefined frequency, to nucleate holes in the domain. For hole nucleation, the sign of the level-set function is changed from negative to positive in the regions where the topological derivative attains minimum negative values. As is evident from the work of Allaire et al. (2005), their topological derivative approach is effective in nucleating holes, but it still does not fully alleviate the dependence on the initial guess. Again, the frequency at which one uses

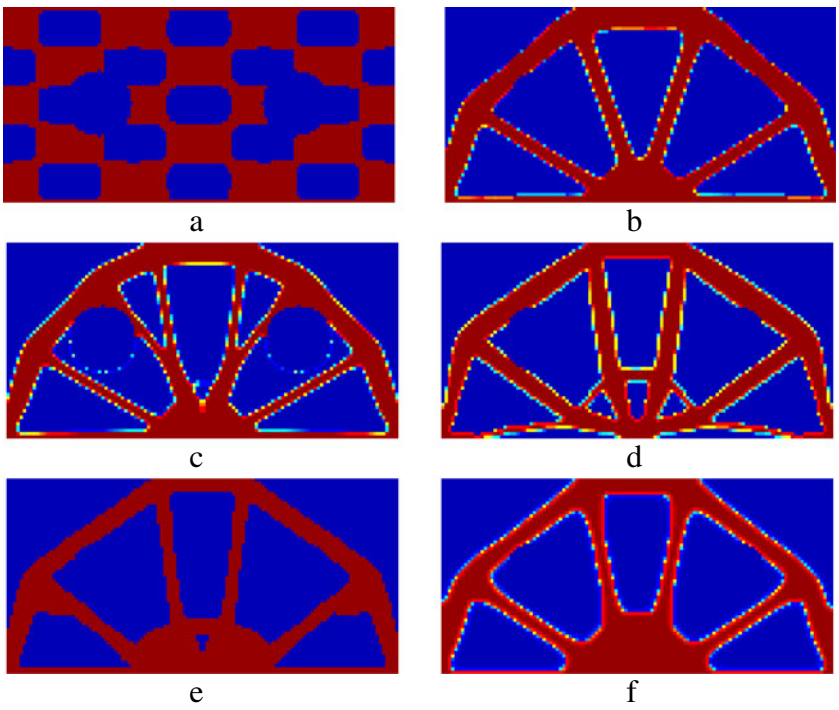

Fig. 11 Converged topologies for bridge with holes problem on a domain discretized using 120×60 mesh. **a** Initial configuration. **b** AJT ($J = 18.6$). **c** DLK ($J = 18.5$). **d** WW ($J = 20.1$). **e** Challis' ($J = 20.5$). **f** TNK ($J = 21.4$)

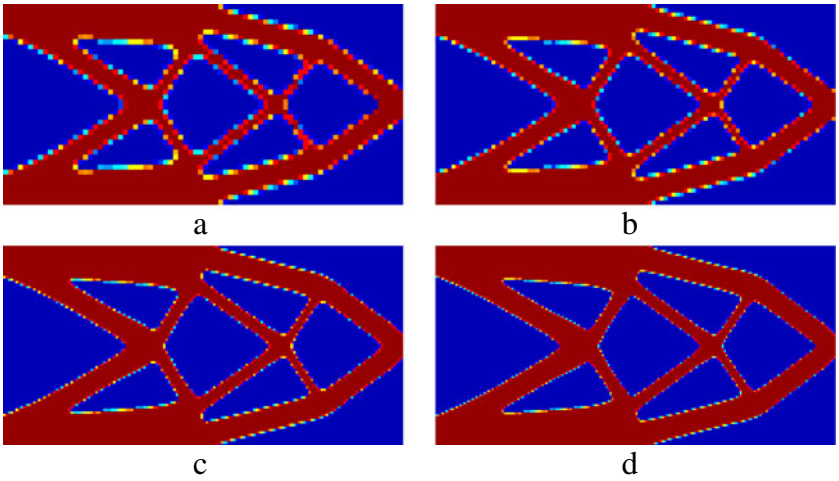

Fig. 12 Study of invariance of the AJT level-set approach to mesh refinement when optimization starts from similar topology of Fig. 8a. Converged configurations for mesh discretizations of **a** 80×40 ($J = 65.8$), **b** 100×50 ($J = 65.9$), **c** 160×80 ($J = 66.0$), and **d** 200×100 ($J = 66.2$)

topological derivatives to nucleate holes is chosen heuristically. If they are employed too often, the domain becomes highly irregular, and if employed sparingly, the algorithm may have already converged to a local minimum which might not be desirable. Some guidelines on choosing the parameters, discussed above, are provided by Allaire et al. (2012).

4.5 Further discussion on the DLK level-set method

In the test problem, we have seen that the DLK approach; which uses sensitivities of the objective function, instead of shape sensitivities, to update the level-set, produces similar configurations when compared to other level-set methods. This method is incapable of generating new holes as other level-set methods, so the converged topology heavily depends on the initial starting configuration. Topological derivatives can be used (discussed before for the AJT level-set approach), to nucleate holes in the design domain and alleviate the dependence on the initial guess to a certain extent. We do not study hole nucleation for the DLK approach in the current work. Here, we first investigate if the DLK level-set approach is invariant to mesh refinement for a similar starting topology. We solve the cantilever beam problem starting with the initial topology, seen in Fig. 8a, for mesh discretizations of 80×40, 100×50, 160×80 and 200×100. Figures 13a–d indicate that the DLK approach produces consistent results for various mesh discretizations and thus it is invariant to mesh refinement when optimization starts from a similar topology.

In the DLK level-set approach, the scaling parameter t is chosen as $h_x/2$ (constrained problem) and the subdivided time step is taken as $t_i = h_x/20$, where h_x is the length of the side of the finite element. In this work, as mentioned before, we chose a slightly larger scaling parameter $t = h_x$ and subdivided time step $t_i = h_x/4$ to speed up the convergence. The convergence is affected if a bigger scaling parameter is chosen. Limits on the scaling parameter t should be provided, similar to the CFL condition, but are not shown in their work.

In this work, the level-set function needs to be reinitialized after each update step; the reason being, that the steepest-descent type updates (24) do not preserve the gradient of the level-set function. The level-set function slope, near the design boundaries, deviates faster from unity in the DLK method than in the AJT method, which necessitates more periodic reinitialization to achieve numerical convergence. Now, consider (18) and (19). By some algebraic manipulations, we can see that:

$$\frac{\partial \bar{J}}{\partial \phi_i} = -\left(\boldsymbol{\varepsilon}(\boldsymbol{u})^T \boldsymbol{C} \boldsymbol{\varepsilon}(\boldsymbol{u}) - \lambda\right) \frac{\partial \rho_e}{\partial \phi_i} \tag{46}$$

Also, from (22) and (23), it is clear that $\frac{\partial \rho_e}{\partial \phi_i} \leq 0$. Let, $\zeta = -\frac{\partial \rho_e}{\partial \phi_i} \geq 0$; thus, (24) can be simplified as:

$$\frac{\phi_i^{n+1} - \phi_i^n}{t} \approx -\bar{\zeta} v_1 \tag{47}$$

where $v_1 = \left(\boldsymbol{\varepsilon}(\boldsymbol{u})^T \boldsymbol{C} \boldsymbol{\varepsilon}(\boldsymbol{u}) - \lambda\right)$ and $\bar{\zeta} = \zeta / \left\| \frac{\partial \bar{J}}{\partial \phi_i} \right\| \geq 0$, $\bar{\zeta} \in [0, 1]$. When compared with the discrete form of the Hamilton-Jacobi equation used in the AJT method (8), i.e.,

$$\frac{\phi_i^{n+1} - \phi_i^n}{t} \approx -v |\nabla \phi_n| \tag{48}$$

we see that (47) and (48) are similar in nature. For both methods, the level-set function propagates in the direction in which the strain energy is minimized.

In this method, the bandwidth of the approximate Heaviside function h is chosen as $d/10$, where d is the length of the diagonal of the finite element. No justification is provided for this choice. Ideally h should be as close to zero as possible (to accurately map the level-set function to the

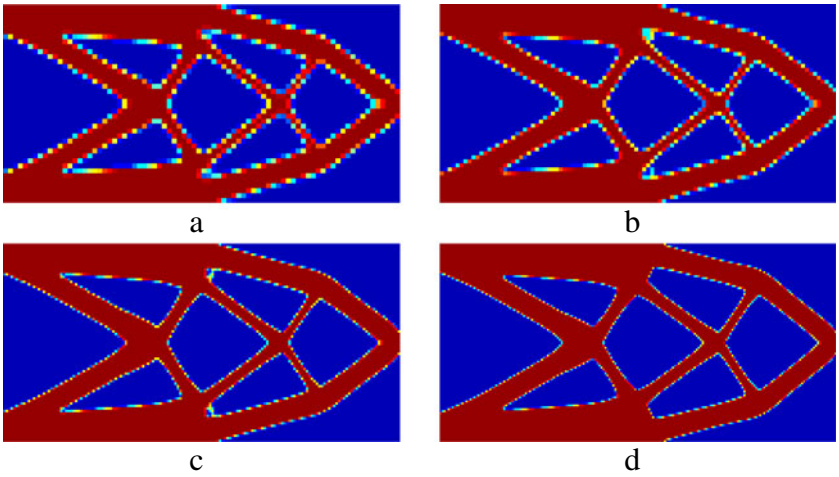

Fig. 13 Study of invariance of the DLK level-set approach to mesh refinement when optimization starts from similar topology. Initial topology is chosen same as Fig. 8a. Converged configurations for mesh discretizations of **a** 80×40 ($J = 64.6$), **b** 100×50 ($J = 65.0$), **c** 160×80 ($J = 65.5$), and **d** 200×100 ($J = 65.9$)

density domain), but h cannot be exactly zero because it will result in infinite gradients (c.f. (22) and (23)). So a scheme needs to be devised to obtain the optimal value of h. Finally, we would like to mention that; since, in this work, we have limited ourselves to compliance minimization problems, we did not investigate the compliant mechanism problem, treated as a multiple constraint optimization problem by applying displacement constraints, in Van Dijk et al.'s work. Effective treatment of multiple constraints is one of the motivations behind Van Dijk et al.'s work. To demonstrate that, Van Dijk et al. (2009) solved the force inverter problem as a multiple constraint problem. Their result for the constrained optimization problem indicates the presence of single node connection and their results for both constrained and unconstrained problems contain tiny voids inside the solid region. This shows that the optimization converges to local minimums, which can be avoided by using regularization algorithms such as filtering. So far Van Dijk et al. have studied the compliance minimization problem and the compliant mechanism problem as a multiple constraint problem. Their method needs to be investigated for other optimization problems such as non-linear elasticity and design dependent load problems, to assess its robustness.

Recently, Van Dijk et al. (2012) published an updated version of their previous method (studied in this work). In their current research, the authors persist with a steepest-descent type updating scheme for the level-set function and look at multiple constraint problems. There are two contrasting differences between the two approaches. First, in the updated version, no reinitialization is used. Second, an exact Heaviside function is used to relate the level-set function and the element densities. It is known that, without some kind of reinitialization or regularization, the level-set function values drift to large absolute values. In order to obtain accurate predicted responses, the authors impose an upper bound on the steepest descent update step for the level-sets and also impose a limit on the size of density change for each level-set update step, both of which are heuristic in nature. Additionally, they utilize heuristic diagonal preconditioner to obtain uniform level-set increments. To deal with the integration of the Heaviside function and its derivatives, in order to obtain the element densities and their sensitivities, the authors define a piecewise linear shape function for Q4 finite elements. Their results show non-physical gray region (compliance minimization results in Van Dijk et al. 2012) and single node connections (compliant mechanism results in Van Dijk et al. 2012), even though good convergence is obtained for the imposed multiple constraints. There are also undesirable oscillations in the convergence history. The authors argue that consistent sensitivity analysis and update scheme lead to good convergence of multi-constrained optimization problem but may also result in numerical artifacts such as excessive gray region and point hinges (similar to density-based topology optimization methods; Bendsøe and Sigmund 2003). The authors tried administering perimeter constraint and density filters to avoid the aforementioned numerical anomalies. Effective treatment of multiple constraints is an important issue which needs to be addressed by the level-set community in the future.

4.6 Further discussion on the WW level-set method

Following the same trend as the previous methods, we first check if the WW method is invariant to mesh refinement for a similar starting topology. We solved the cantilever beam problem, using the initial guess in Fig. 8a, for mesh discretizations of 80×40 and 100×50. The result for the 120×60 mesh is already shown in Fig. 8d. We could not run the problem for meshes larger than 120×60, for reasons which will be discussed later in this section. Results (Figs. 14a–b and Fig. 8d) suggest that the WW level-set method is

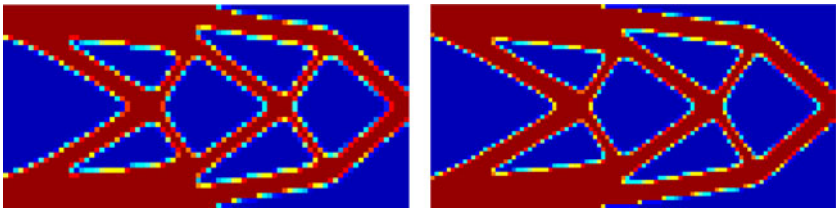

Fig. 14 Study of invariance of the WW level-set approach to mesh refinement for similar starting topology. Figure 8a is the chosen starting topology. Converged configurations for mesh discretizations of **a** 80×40 ($J = 65.8$) and **b** 100×50 ($J = 66.3$)

also invariant to mesh refinement when the optimization algorithm starts from a similar topology.

To investigate the issue of sensitivity of the final topology to the initial chosen configuration, we ran the cantilever beam problem with two different initial configurations (Figs. 15a and 16a). The corresponding converged topologies (Figs. 15f and 16b) support the author's claim of hole nucleation; however, lack of a unique converged topology (c.f. Figs. 8d, 9d, 15f and 16b) for various initial guesses confirms that dependence on the initial guess has not been fully resolved. The method still converges to local minimums, dictated by the starting topology.

In the present approach, Wang and Wang (2006) used radial basis functions to parameterize the level-set function. Our implementation of the WW approach suggests that although the infinite smoothness of MQ splines helps maintain smoothness of $\boldsymbol{N}^T(\boldsymbol{x})$ (c.f. (30)), the level-set function grows to very high absolute values because of the rapid growth in $\boldsymbol{\alpha}(t)$. To observe this, consider Fig. 17; which shows the level-set function for the converged configuration in Fig. 8d. Towards the end of optimization, at some locations across the design boundaries, the level-set function (Fig. 17b) varies in the order of $+10^{24}$ to -10^{24} (much higher at some other locations). Such unbounded growth and high variation implies that the boundary is too steep (hence high gradients) and, thus, obtaining an accurate approximation of the normal at the design interface is difficult. This might cause the algorithm to converge to incorrect results. Smooth radial basis functions do alleviate the problem of high gradients to a certain extent, by providing some sort of smoothness to the level-set function, without which, the algorithm does not converge.

In the WW approach, a new scheme is introduced to extend the advection velocity field, defined on the front using shape derivatives, to the entire design domain. In order to provide a physically meaningful extension velocity, they assumed a strain field $\boldsymbol{\varepsilon}(\boldsymbol{u}) = 0$, resulting in a strain energy of $\boldsymbol{\varepsilon}^T\boldsymbol{C}^*\boldsymbol{\varepsilon} = 0$, for $\phi(\boldsymbol{x}) > \delta$. This assumption adds little value when we are using an Ersatz material approach, since in the region $\phi > 0$ (void region) we assume $\boldsymbol{C}^* \approx 0$ which results in a strain energy of $\boldsymbol{\varepsilon}^T\boldsymbol{C}^*\boldsymbol{\varepsilon} \approx 0$. The authors also smooth the advection velocity near the design interface, citing the reason that the advection velocity is discontinuous at the boundaries. It should be noted that the advection velocity is C^0 continuous (c.f. (34)). The smoothing of the advection velocity helps bring down the gradients to a certain extent, but, high inaccurate gradients persist in some regions, especially the region around the point of application of the load. Such high values of level-set function can be attributed to the fact that the WW method does not utilize any regularization schemes (for example, reinitialization), other than velocity smoothing, to control the gradients of the level-set function near the design boundaries. When we tried to periodically reinitialize the level-set function in the WW scheme, we were able to control the magnitude of the gradients (as expected) but it resulted in the loss of hole nucleation capability.

Wang and Wang (2006) argued that reinitialization is computationally expensive and time consuming, which is true to a certain extent, but this cost is minimal compared to the solution of the Hamilton-Jacobi equation using multi-quadratic radial basis functions. Multi-quadratic splines produce a dense interpolation matrix $\boldsymbol{H}$ which is known to be ill-conditioned. So, the design update (33) is very expensive since it requires inversion of a dense matrix. We could run examples only up to a mesh discretization of 120×60; which converged within a reasonable time frame. Finer meshes either take too long to converge (more than a few hours) or the system runs out of memory.[7] Many techniques are available to efficiently handle dense, ill-conditioned matrices such as the domain decomposition method, fast multi-pole method and pre-conditioning (Buhmann 2004). In their work, in order to speed up the convergence Wang et al. chose time steps of 10^{-3} or 10^{-4} which is much larger than the CFL time steps (the CFL time step is of the order of 10^{-5}, 10^{-6} for 40×20, 120×60 meshes, respectively). Although rapid convergence can be achieved by using bigger time steps, it creates instability in the system due to large accumulated errors.

Finally, we also investigated the influence of shape parameter c, which controls the flatness of the radial basis

[7] All the numerical problems were performed on Intel(R) Core 2 Quad, 2.49 GHz processor and 8 GB RAM running MATLAB R2009a.

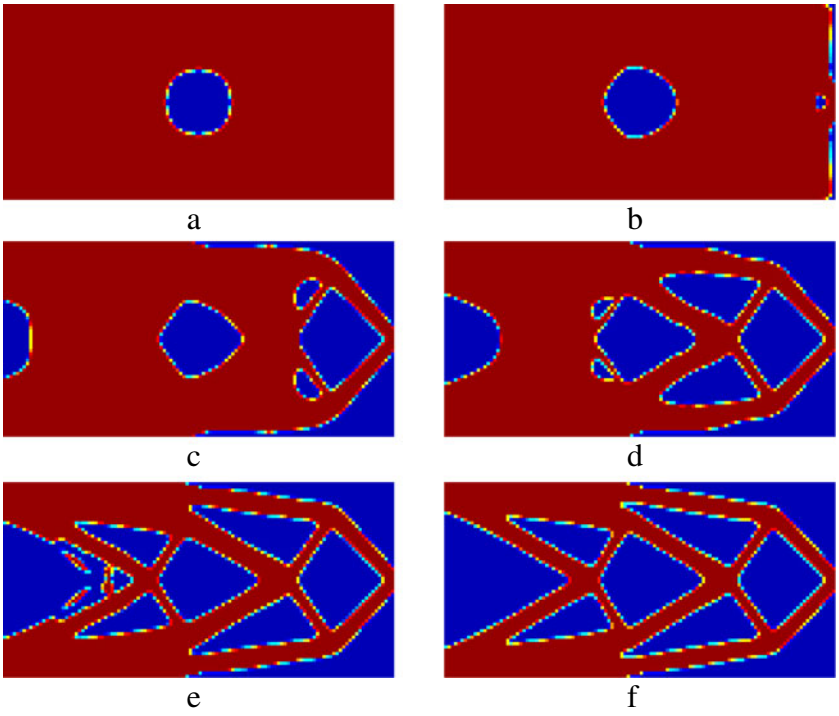

Fig. 15 Evolution of topology for curved cantilever beam problem starting with initial topology **a** for the WW approach on a 120 × 60 mesh. **b** Iteration 56. **c** Iteration 80. **d** Iteration 85. **e** Iteration 92. **f** Converged topology

function, on the optimization algorithm. We varied c in the range $10^{-5} - 10^{-1}$ for mesh discretization of 80 × 40 and the initial guess shown in Fig. 8a. Our study (Table 2) shows that the condition number of $\boldsymbol{H}$ increases with c, indicating an increase in instability in the system. The compliances are approximately the same with no discernible trend. Visually, the converged topologies are all similar to the test problem solution for the WW method (Fig. 8d). We did observe that for $c = 10^{-1}$, the condition number of $\boldsymbol{H}$ becomes too high and thus the algorithm fails to convergence. This sets an upper limit on the choice of c. Similar results were observed for other mesh discretizations.

4.7 Further discussion on Challis' level-set method

In its current form, Challis' algorithm possesses some limitations. Her implementation takes a long time to converge if the mesh discretization is greater than 5000 elements. Because her original code was developed for educational purpose, justifiably little effort was made on the part of the author to make it more efficient. We have alleviated this problem by using sparse matrix assembly as mentioned before. Similar to the AJT method, in Challis' implementation, it is difficult to estimate the optimum number of Hamilton-Jacobi equation update steps that need to be performed for every finite element update. There is a trade off between accuracy and computational time. Challis uses the MATLAB function `bwdist` for reinitialization which excessively smooths the level-set function. It is also not possible to control the degree of smoothness with `bwdist`. Other approaches, such as the one used in the AJT method, where (16) is used for reinitialization, although computationally more expensive, can provide the desired control over smoothness. As indicated earlier, in Challis' approach the traditional Hamilton-Jacobi equation (c.f. (8)) is modified to include topological derivatives which aid in the generation of holes. Frequency of reinitialization is a significant issue with regards to hole nucleation. In Challis' method, reinitializing the level-set function too often neutralizes the effect of topological derivatives and thus, the hole generation capability is lost. Therefore, it is vital that a suitable reinitialization frequency is established, which not

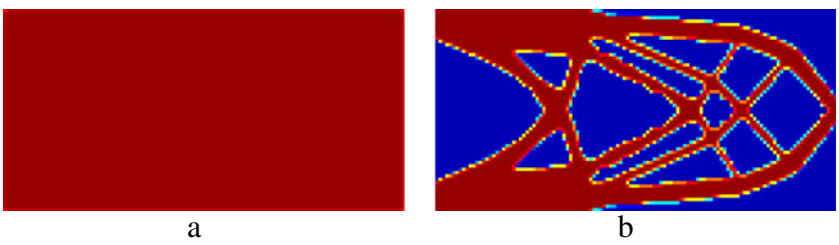

Fig. 16 Different initial topology for the WW approach on a 120 × 60 mesh. **a** Initial guess. **b** Converged configuration

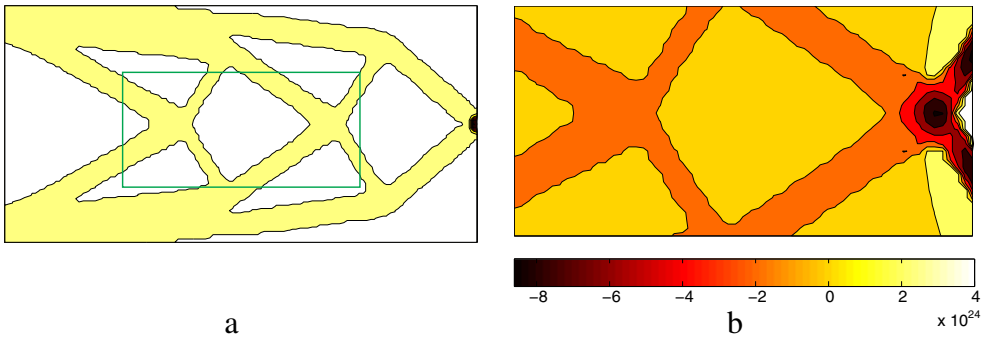

Fig. 17 Level-set function corresponding to the converged topology in Fig. 8d. **a** Level-set function. **b** Zoomed in section

only keeps the level-set function gradients near the design boundaries under control, but also does not hamper hole nucleation.

In Challis' approach, positive constant w controls the influence of topological derivatives. We next examine the influence of w on the optimization using the cantilever beam problem Fig. 7. Parameter w is varied in the set $\{2, 3, 4, 6, 8, 10\}$. The domain discretization is fixed to 80×40 and the other parameters are kept constant ($V_{max} = \texttt{volRec} = 0.45$, $\texttt{stepLength} = 2$, $\texttt{numReinit} = 4$). It can be seen from Fig. 18 that parameter w significantly influences the final topology. For $w = \{2, 3, 4\}$, the topologies are visually similar.

The parameter w is also mesh dependent and the next study confirms this statement. We keep w constant at 3, all other parameters are kept the same as they were in the last study, and we vary the mesh discretization. We observe that the final configurations are different for different mesh discretizations (Fig. 19). These two studies indicate that w significantly influences the optimization algorithm. A smaller value prevents new holes from nucleating and a larger value causes the topological derivatives to dominate, producing too many holes. More work needs to be carried out to arrive at an optimal value for w.

In this approach, shape and topological sensitivities are smoothed after each state equation solution over the entire domain. Explicit sensitivity smoothing is typically employed to reduce the probability of convergence to a local minimum. But, care must be taken when applying such smoothing techniques, because it affects the hole nucleation process and also the rate of convergence of the algorithm.

In Challis' approach, a border of void elements around the design domain is included. The author claimed that they are necessary to represent the boundary of the structure accurately; which actually aids the algorithm to converge. This approach has been applied to compliance minimization problems and needs to be tested for other problems such as compliant mechanisms, design dependent loads and non-linear elasticity problems, for robustness.

4.8 Further discussion on the TNK phase-field method

The phase-field method by Takezawa et al. (2010) utilizes a time dependent reaction-diffusion equation, known as the Allen-Cahn equation, for the evolution of topologies. The sensitivity of the objective function, employed extensively in density methods, is used to define a double well potential function which is a part of the evolution equation. Unlike level-set methods, the phase-field method eliminates the need for reinitialization, which can be costly. This method has been verified for minimum compliance, compliant mechanism and eigenfrequency maximization problems. Problems such as nonlinear elasticity, design dependent loads and minimum stress are yet to be explored.

The phase-field method performed well for the test problem shown earlier and produced expected topologies. As shown in the cantilever beam problem, like level-set methods, the phase-field method does not have an embedded hole generation mechanism and thus the final topologies are influenced by the initial topology. Takezawa et al. suggest the use of topological derivatives to alleviate this problem which is similar to the approach in level-set methods

Table 2 Influence of shape parameter, c, on the WW level-set method for 80×40 mesh

c	Compliance (J)	Converged volume fraction	Condition number of $\boldsymbol{H}$ (c.f. (27), (28))	Iterations
10^{-5}	66.4	0.45	2.67×10^5	93
10^{-4}	65.8	0.45	2.70×10^5	147
10^{-3}	65.8	0.45	2.94×10^5	212
10^{-2}	65.7	0.45	7.97×10^5	298
10^{-1}	–	–	1.06×10^{12}	No convergence

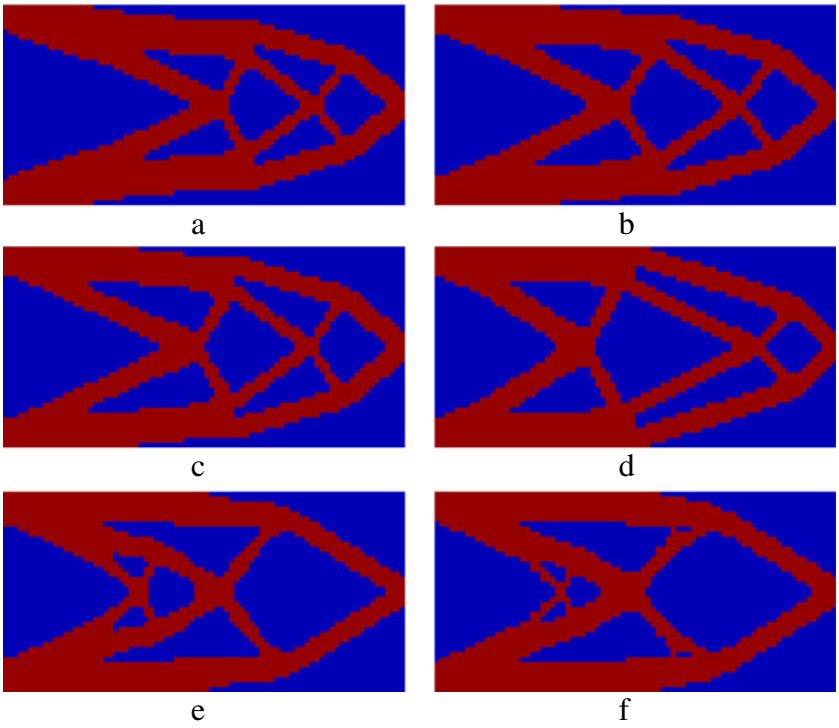

Fig. 18 Study of the influence of parameter w on Challis' approach using cantilever beam problem on a 80×40 mesh. Initial configuration is a fully solid domain. Converged configurations for **a** $w = 2$ ($J = 72.1$), **b** $w = 3$ ($J = 68.6$), **c** $w = 4$ ($J = 70.0$), **d** $w = 6$ ($J = 68.4$), **e** $w = 8$ ($J = 71.2$), and **f** $w = 10$ ($J = 70.6$)

(Allaire et al. 2005). We did not investigate the use of topological derivatives in the phase-field method to generate holes. From Takezawa et al.'s work (Takezawa et al. 2010), it is evident that the use of topological derivatives is a feasible option to nucleate holes. However, further work is required to verify the accuracy of this approach and more test problems need to be investigated to establish its robustness.

The diffusion coefficient, κ, plays a critical role in the phase-field method. We investigate the effects of κ on the optimization process using the cantilever beam problem. For the first study, the domain discretization is fixed at 160×80 elements; a volume fraction of 0.45 is prescribed and κ is varied. Figure 20a is chosen as the initial configuration. Optimization is performed for $\kappa = 0.5 \times 10^{-5}$, 2×10^{-5} and 5×10^{-5}. From Fig. 20b–d, it is evident that as κ increases, the thickness of the diffuse interface increases. The percentage of total elements in the diffuse interface (Fourth column in Table 3), gives a general idea about the diffuse interface thickness. Design boundary becomes increasingly fuzzy. Also, the number of holes decreases with increasing κ. Thus, κ also affects the perimeter of the final configuration.

For the next study, we fix κ to 1×10^{-5} and vary the mesh discretizations. The initial guess is kept the same as in the previous study. We see that for a particular κ (1×10^{-5} in this case), too coarse of a mesh discretization (Figs. 21a

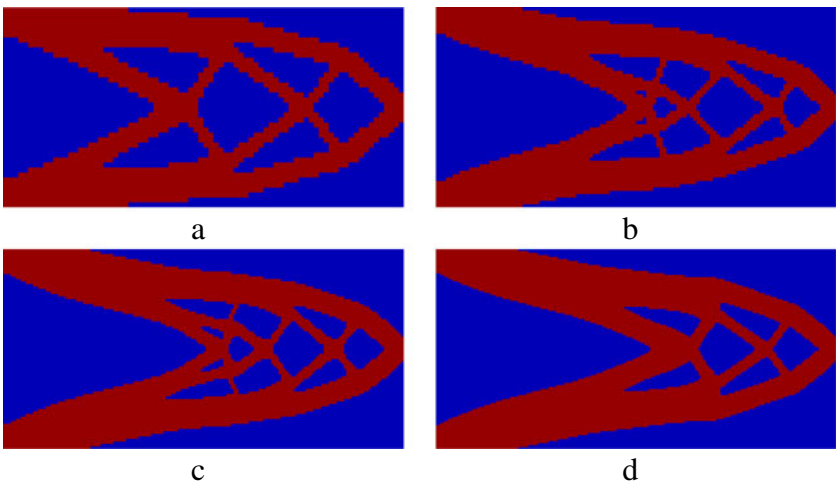

Fig. 19 Mesh refinement study with $w = 3$ for Challis' approach. Initial configuration is a fully solid domain. Converged configurations on mesh discretization of **a** 80×40 ($J = 68.6$), **b** 120×60 ($J = 72.7$), **c** 160×80 ($J = 73.0$), **d** 200×100 ($J = 73.2$)

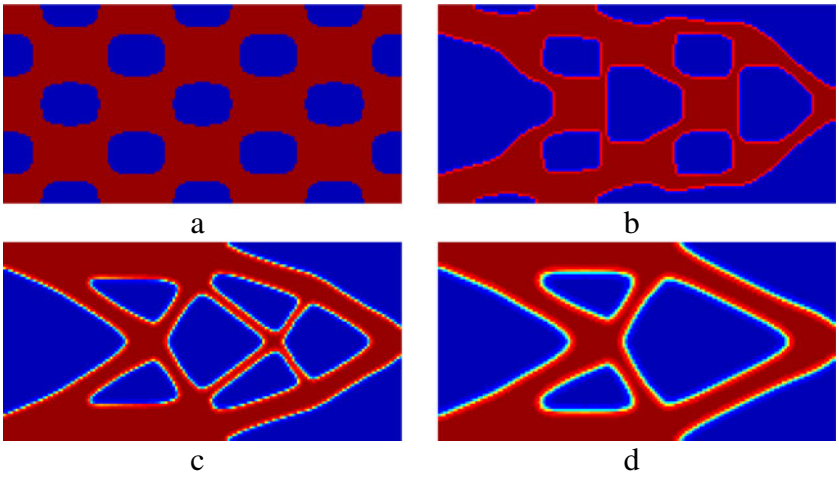

Fig. 20 Study of the influence of diffusion coefficients κ on the TNK phase-field approach. Mesh discretization is 160×80 and **a** is the starting configuration. Converged configurations for **b** $\kappa = 0.5 \times 10^{-5}$, **c** $\kappa = 2 \times 10^{-5}$, and **d** $\kappa = 5 \times 10^{-5}$

and b) hinders the optimization and the algorithm stops prematurely, which is evident from the final volume fractions in Table 4. Finer discretizations in the range 160×80 and 200×100 (Fig. 21c, d) seem to be more ideal for $\kappa = 1 \times 10^{-5}$ (least compliance).

From these two studies it is clear that the choice of κ is mesh dependent. It not only controls the thickness of the diffuse interface but also the number of holes, thus perimeter, of the final configuration. If κ is too small the resulting thickness of the diffuse interface is too small and thus the evolution of the topology is hindered. On the other hand, if κ is too big, then there is excess gray region and fewer holes in the converged topology (Fig. 22). Our numerical experimentation shows that the ideal choice of κ is one which produces topologies with approximately three-to-four elements in the diffuse interface.

To conclude, the diffusion coefficient, κ, needs to be scaled appropriately, when the mesh discretization is varied, to get consistent designs. It should also be noted that, in the interpolation function (41) (same as SIMP model), the power p also affects the gray region. A penalty, p, greater than or equal to 3 is recommended in the SIMP model.

The phase-field method discussed here (TNK method) is similar to density-based methods in many aspects. Both methods have the same domain representation and their optimization algorithms are primarily driven by sensitivity information. Material interpolation schemes such as SIMP, RAMP (Stolpe and Svanberg 2001; Bendsøe and Sigmund 2003) and ECP (Yoon and Kim 2005; Yoon et al. 2007, 2008), are equally applicable to both. The main difference between the two methods is in the updating algorithms they employ. Mathematical programming algorithms; such as, Method of Moving Asymptotes (MMA, Svanberg 1987), Optimality Criteria (OC, Bendsøe and Sigmund 2003), Sequential Linear Programming (SLP), Sequential Quadratic Programming (SQP), CONvex LINearization approximations (CONLIN, Fleury and Braibant 1986) have been applied to density-based methods. Additional techniques such as filtering, perimeter constraint (Bendsøe and Sigmund 2003) and manufacturing constraints (Kosaka and Swan 1999; Almeida et al. 2010) are used to regularize the design. In the TNK method, the design is updated using the Allen-Cahn equation (c.f. (42, 43)). Perimeter constraint is built-in to the updating scheme and can be controlled via the diffusion coefficient, κ. Moreover, the double well potential function (43) has a regulating effect as it drives the design towards a 0-1 solution.

Finally, Table 5 summarizes the key features of the differential equation-driven methods discussed in this study.

5 Conclusions

In this work, we study four level-set methods and one phase-field method. The AJT level-set method (Allaire et al. 2004) is the first method we analyze. In this method, shape

Table 3 Influence of diffusion coefficient, κ, on the TNK phase-field method for a fixed 160×80 mesh and $V_{max} = 0.45$ (c.f. Fig. 20)

κ	Compliance (J)	Converged volume fraction	Elements in the diffuse interface ($0.01 < \phi < 0.99$)
0.5×10^{-5}	87.6	0.45	13.8 %
2.0×10^{-5}	71.9	0.45	27.6 %
5.0×10^{-5}	74.7	0.45	33.0 %

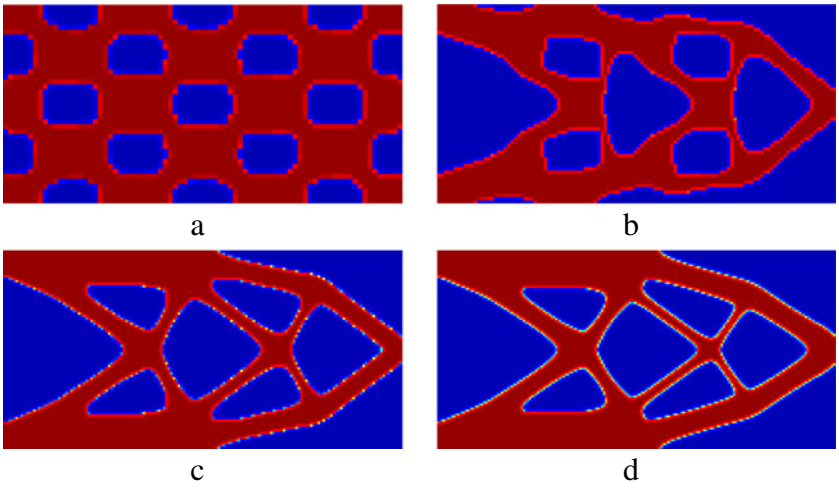

Fig. 21 Cantilever beam problem solved on different mesh discretizations with diffusion coefficient $\kappa = 1 \times 10^{-5}$. Figure 20a is choosen as the initial guess. Converged topologies for mesh discretizations of **a** 80×40, **b** 120×60, **c** 160×80, and **d** 200×100

derivatives are combined with the Hamilton-Jacobi equation for the design front propagation. The second method we look at is the DLK level-set method (Van Dijk et al. 2009) in which the objective function sensitivity is used in a steepest-descent type update scheme. The WW level-set method (Wang and Wang 2006) transforms the Hamilton-Jacobi equation into a set of ordinary differential equations (ODEs) using multi-quadratic radial basis functions. The ODEs are solved using Euler's method. Challis' level-set method (Challis 2010) utilizes Burger et al. (Burger et al. 2004) approach of modifying the Hamilton-Jacobi equation to include topological sensitivity to nucleate holes in the design domain. Finally, we also study the TNK phase-field method (Takezawa et al. 2010) for structural topology optimization. The design domain is represented in terms of a phase-field function and evolved using the Allen-Cahn equation; which utilizes objective function sensitivity.

Our study shows that, in all five methods, the final topologies are dependent on the starting initial configurations. Although, the WW method and Challis' method nucleate holes in the design domain, these methods still possess the initial configuration dependency. The AJT method produces designs which are invariant to mesh refinement when optimization starts from a similar topology i.e. starting from a similar initial topology, the method should produce designs of similar topological complexity for different mesh discretizations. In the AJT method, certain parameters such as the number of Hamilton-Jacobi updates per state equation solution, frequency of reinitialization and number of times the reinitialization equation is solved, are chosen heuristically. A physically meaningful scheme needs to be devised which can estimate the optimum parameter values. The DLK method also produces designs which are mesh invariant for similar starting topology but requires very frequent reinitialization for the algorithm to converge, making it computationally expensive and resulting in a slow rate of convergence. Reinitialization is required frequently, because the steepest-descent type update (24) used in the DLK method does not preserve the magnitude of the gradient of the level-set function. The slope of the level-set function needs to be controlled near the design interface for convergence. Unlike other level-set methods,

Table 4 Study of affect of diffusion coefficient ($\kappa = 1 \times 10^{-5}$ with variations in mesh discretization on the TNK phase-field method (c.f. Fig. 21). Volume fraction, $V_{max} = 0.45$, is imposed on the system

Mesh discretization	Compliance (J)	Converged volume fraction
80×40	123.9	0.66
120×60	78.5	0.46
160×80	70.7	0.45
200×100	70.6	0.45

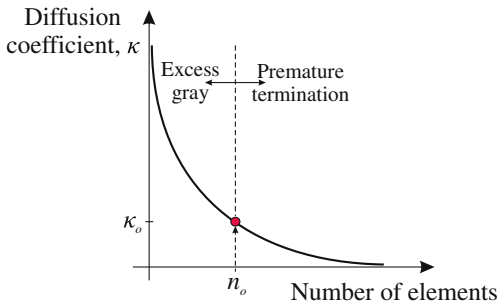

Fig. 22 Qualitative illustration of the variation of the choice of diffusion coefficient κ versus the mesh refinement. For a particular choice of mesh refinement n_o, if κ_o represents the ideal choice of κ then any $\kappa > \kappa_o$ will result in lesser holes and excess gray region in the converged configuration. On the other hand if $\kappa < \kappa_o$ then the algorithm stops prematurely. Here, the ideal choice of κ is defined as the value which produces topologies with approximately three-to-four elements in the diffuse interface

Table 5 Summary of the differential equation-driven methods for two-dimensional topology optimization discussed in this study

Authors	Acronym	Method classification	Evolution equation	Reinitialization	Inherent hole nucleation [9]	Dependence on initial guess	Remarks
Allaire, Jouve and Toader (2004)	AJT	Level-set method	Hamilton-Jacobi	Yes	No	Yes	• Parameters, such as, number of update steps of Hamilton-Jacobi equation, frequency of reinitialization, and number of solution steps of reinitialization equation chosen heuristically.
Van Dijk, Langelaar and Van Keulen (2009)	DLK	Level-set method	Steepest-descent	Yes	No	Yes	• Requires frequent reinitialization to maintain signed distance nature of the level-set function at all times for convergence which makes the algorithm computationally expensive and slow.
Wang and Wang (2006)	WW	Level-set method	Hamilton-Jacobi	No	Yes	Yes	• Elimination of reinitialization and adoption of smoothed naturally extended velocities aids the creation of new holes. • Requires frequent inversion of dense matrices which makes the algorithm computationally very expensive.
Challis (2010)	–	Level-set method	Hamilton-Jacobi	Yes	Yes	Yes	• Nucleates holes due to the use of modified Hamilton-Jacobi equation which includes topological derivatives but does not alleviate dependence on initial guess. • Introduces mesh dependent parameter, w, which controls the influence of topological derivatives.
Takezawa, Nishiwaki and Kitamura (2010)	TNK	Phase-field method	Allen-Cahn	No	No	Yes	• No reinitialization needed. • Diffusion coefficient, κ, needs to be scaled with mesh refinement for mesh independent designs.

[9]For methods which do not have any inherent hole nucleation mechanism, topological derivatives can be used to nucleate holes in the design domain

the WW method does not periodically reinitialize the level-set function, to save computational cost, and it also aids in the hole nucleation process. But, this also causes the level-set function and its gradients to grow to large values, making accurate approximation of the normal at design boundaries difficult. The WW method also produces dense matrices which need to be inverted frequently, rendering them computationally very expensive. Challis' method possesses a built-in hole nucleation mechanism, because of the modified Hamilton-Jacobi equation which incorporates topological derivatives. But, the final topologies depend on the choice of mesh-dependent parameter w; which determines the influence of topological derivatives. The TNK phase-field method does not require the phase-field function to be a signed distance function, so no reinitialization is needed. In this method, the diffusion coefficient, κ; which controls the thickness of diffuse interface and the perimeter of the final configuration, is mesh dependent and needs to be scaled appropriately for meshes of different discretization. It should be noted that, of all the five methods we studied, only Challis' method enforces black and white solutions.

In this work, we focused on two-dimensional optimization problems for which hole nucleation is a challenge. For the three-dimensional case, Allaire et al. (2004) have shown that the traditional level-set approach of using an advection equation with shape derivatives is able to nucleate new holes in the domain due to the pinching of thin walls. Also, we limited ourselves to compliance minimization problems for simplicity. Most methods in the literature tend to perform relatively well in the case of compliance minimization and thus may appear to be similarly effective. Methods which produce similar results for compliance minimization might exhibit drastically different behavior for other objectives, such as compliant mechanism, stress criterion and nonlinear elasticity. Only when these methods are tested against objectives other than compliance can one ascertain the actual robustness of the method.

We would like to point out that the evolution equations for the level-set methods and phase-field method that we have examined in this work can be regarded as some sort of steepest decent method. In the case of compliance, the algorithms strive to minimize the strain energy in the system by placing more material at high strain energy locations. Thus, the differential equation-driven methods follow the same design philosophy as the density based methods for topology optimization.

Nomenclature

$\boldsymbol{u}$	admissible displacement field satisfying equilibrium
$\boldsymbol{\varepsilon}$	linearized strain field
$\boldsymbol{f}$	applied body force
$\boldsymbol{g}$	surface loads
J	objective function
$\bar{J}$	effective objective function
λ	Lagrangian multiplier used to reformulate the objective function
$\boldsymbol{C}$	elasticity tensor for solid phase
$\boldsymbol{C}^*$	effective elasticity tensor for the entire design domain
ϕ	design function, level-set or phase-field
Ω	admissible design for the optimization problem
D	working domain consisting of all admissible shapes Ω
$\boldsymbol{F}$	discretized global force vector
$\boldsymbol{U}$	discretized global displacement vector
$\boldsymbol{\rho}$	density array
$\boldsymbol{V}$	array of the fractional areas of elements
V_{max}	prescribed volume fraction
Ω_1	solid phase domain in the TNK phase-field method
Ω_0	void phase domain in the TNK phase-field method
ξ	diffuse interface
ρ_e	element densit
k_{min}	scaling factor to determine lowest limit of $\boldsymbol{C}^*$
v	advection velocity for Hamilton-Jacobi equation obtained through sensitivity analysis
$v_{i,j}$	v for the nth iteration at node located at $\boldsymbol{x}_{i,j}$
$\phi^n_{i,j}$	ϕ for the nth iteration at node located at $\boldsymbol{x}_{i,j}$
Δt	time step
$\boldsymbol{Q}$	Lagrangian multiplier vector for the equilibrium constraint
$\boldsymbol{R}$	residual vector
N_i	radial basis function
c_i	constant shape parameter for multi-quadratic splines
α_i	weights for the radial basis functions
r_{min}	filter radius to smooth advection velocity in the WW level-set scheme
$g(\boldsymbol{x})$	topological sensitivity
w	positive weight for $g(\boldsymbol{x})$
$f(\phi)$	double well potential function
$\bar{J}'$	sensitivity of the effective objective function
η	scaling constant in the TNK phase-field method
κ	diffusion coefficient
Δx	nodal distance in x direction
Δy	nodal distance in y direction

References

Allaire G, Jouve F (2005) A level-set method for vibration and multiple loads structural optimization. Comput Methods Appl Mech Eng 194:3269–3290

Allaire G, Jouve F (2008) Minimum stress optimal design with the level set method. Eng Anal Bound Elem 32:909–918
Allaire G, Kohn RV (1993) Optimal design for minimum weight and compliance in plane stress using extremal micostructures. EUR J MECH A-/Solids 12(6):839–878
Allaire G, Pantz O (2006) Structural optimization with FreeFem++. Struct Multidiscip Optim 32(3):173–181
Allaire G, Jouve F, Toader A-M (2002) A level set method for shape optimization. Comptes Rendus Mathematique 12:1125–1130
Allaire G, Jouve F, Toader A-M (2004) Structural optimization using sensitivity analysis and a level-set method. J Comput Phys 194:363–393
Allaire G, de Gournay F, Jouve F, Toader A-M (2005) Structural optimization using topological and shape sensitivity via a level set method. Control Cybern 34(1):59–80
Allaire G, Karrman A, Michailidis G (2012) Scilab code manual. http://www.cmap.polytechnique.fr/allaire/levelset_en.html
Allen SM, Cahn JW (1979) A microscopic theory for antiphase boundary motion and its application to antiphase domain coarsening. Acta Metall 27:1085–1095
Almeida SRM, Paulino GH, Silva ECN (2010) Layout and material gradation in topology optimization of functionally graded structures: a global-local approach. Struct Multidiscip Optim 42(6):855–868
Amstutz S, Andrä H (2006) A new algorithm for topology optimization using a level-set method. J Comput Phys 216:573–588
Aranson IS, Kalatsky VA, Vinokur VM (2000) Continuum field description of crack propagation. Phys Rev Lett 85(1):118–121
Belytschko T, Xiao SP, Parimi C (2003) Topology optimization with implicit functions and regularization. Int J Numer Methods Eng 57:1177–1196
Bendsøe MP (1989) Optimal shape design as a material distribution problem. Struct Optim 1:193–202
Bendsøe MP, Kikuchi N (1988) Generating optimal topologies in structural design using a homogenization method. Comput Methods Appl Mech Eng 71(2):197–224
Bendsøe MP, Sigmund O (1999) Material interpolation schemes in topology optimization. Arch Appl Mech 69(9–10):635–654
Bendsøe MP, Sigmund O (2003) Topology optimization - theory, methods and applications. Springer, New York
Bourdin B, Chambolle A (2003) Design-dependent loads in topology optimization. ESAIM - Control Optim Calc Var 9:19–48
Buhmann MD (2004) Radial basis functions: Theory and implementations. Cambridge monographs on applied and computational mathematics, vol 12. Cambridge University Press
Burger M, Stainko R (2006) Phase-field relaxation of topology optimization with local stress constraints. SIAM J Control Optim 45(4):1447–1466
Burger M, Hackl B, Ring W (2004) Incorporating topological derivatives into level set methods. J Comput Phys 194:344–362
Cahn JW, Hillard JE (1958) Free energy of a nonuniform system. I. Interfacial energy. J Chem Phys 28:258–267
Céa J, Garreau S, Guillaume P, Masmoudi M (2000) The shape and topological optimizations connection. Comput Methods Appl Mech Eng 188(4):713–726
Challis VJ (2010) A discrete level-set topology optimization code written in Matlab. Struct Multidiscip Optim 41(3):453–464
Challis VJ, Guest JK (2009) Level-set topology optimization of fluids in Stokes flow. Int J Numer Methods Eng 79(10):1284–1308
Challis VJ, Roberts AP, Wilkins AH (2008) Design of three dimensional isotropic microstructures for maximized stiffness and conductivity. Int J Solids Struct 45(14–15):4130–4146
Challis VJ, Guest JK, Grotowski JF, Roberts AP (2012) Computationally generated cross-property bounds for stiffness and fluid permeability using topology optimization. Int J Solids Struct 49(23–24):3397–3408
Chang YC, Hou TY, Merriman B, Osher S (1996) A level set formulation of Eulerian interface capturing methods for incompressible fluid flows. J Comput Phys 124:449–464
Chopp DL (1993) Computing minimal surfaces via level set curvature flow. J Comput Phys 106:77–91
Cunha AL (2004) A fully Eulerian method for shape optimization with application to Navier-Stokes flows. PhD thesis. Carnegie Mellon University
De Ruiter MJ, Van Keulen F (2004) Topology optimization using a topology description function. Struct Multidiscip Optim 26(6):406–416
Duan XB, Ma YC, Zhang R (2008) Shape-topology optimization for Navier-Stokes problem using variational level set method. J Comput Appl Math 222(2):487–499
Eschenauer H, Kobelev VV, Schumacher A (1994) Bubble method for topology and shape optimization of structures. Struct Optim 8(1):42–51
Fleury C, Braibant V (1986) Structural optimization: a new dual mehod using mixed variables. Int J Numer Methods Eng 23(3):409–428
Gain AL, Paulino GH (2012) Phase-field based topology optimization with polygonal elements: a finite volume approach for the evolution equation. Struct Multidiscip Optim 46(3):327–342
Garreau S, Guillaume P, Masmoudi M (2001) The topological asymptotic for PDE systems: The elasticity case. SIAM J Control Optim 39(6):1756–1778
Ha SH, Cho S (2005) Topological shape optimization of heat conduction problems using level set approach. Numer Heat Transf Part B: Fundam 48(1):67–88
Haber E (2004) A multilevel, level-set method for optimizing eigenvalues in shape design problems. J Comput Phys 198(2):518–534
He L, Kao CY, Osher S (2007) Incorporating topological derivatives into shape derivatives based level set methods. J Comput Phys 225:891–909
Ho HS, Wang MY, Zhou M (2013) Parametric structural optimization with dynamic knot RBFs and partition of unity method. Struct Multidiscip Optim 47(3):353-365
Iga A, Nishiwaki S, Izui K, Yoshimura M (2009) Topology optimization for thermal conductors considering design-dependent effects, including heat conduction and convection. Int J Heat Mass Transfer 52(11-12):2721–2732
Kao CY, Osher S, Yablonovitch E (2005) Maximizing band gaps in two-dimensional photonic crystals by using level set methods. Appl Phys B Lasers Opt 81(2):235–244
Kawamoto A, Matsumori T, Yamasaki S, Nomura T, Kondoh T, Nishiwaki S (2011) Heaviside projection based topology optimization by a PDE-filtered scalar function. Struct Multidiscip Optim 44(1):19–24
Kim MG, Ha SH, Cho S (2009) Level set-based topological shape optimization of nonlinear heat conduction problems using topological derivatives. Mech Base Des Struct Mach 37(4):550–582
Kobayashi R (1993) Modeling and numerical simulations of dendritic crystal growth. Phys D Nonlinear Phenom 63(3–4):410–423
Kosaka I, Swan CC (1999) A symmetry reduction method for continuum structural topology optimization. Comput Struct 70(1):47–61
Kreissl S, Maute K (2012) Levelset based fluid topology optimization using the extended finite element method. Struct Multidiscip Optim. doi:10.1007/s00158-012-0782-8

Kreissl S, Pingen G, Maute K (2011) An explicit level set approach for generalized shape optimization of fluids with lattice Boltzmann method. Int J Numer Methods Fluids 65:496–519
Lui Z, Korvink JG, Huang R (2005) Structure topology optimization: fully coupled level set method via FEMLAB. Struct Multidiscip Optim 29(6):407–417
Luo Z, Tong L, Wang MY, Wang S (2007) Shape and topology optimization of compliant mechanisms using a parameterization level set method. J Comput Phys 227(1):680–705
Luo J, Luo Z, Chen L, Tong L, Wang MY (2008a) A semi-implicit level set method for structural shape and topology optimization. J Comput Phys 227(11):5561–5581
Luo J, Luo Z, Chen L, Tong L, Wang MY (2008b) A new level set method for systematic design of hinge-free compliant mechanisms. Comput Methods Appl Mech Eng 198(2):318–331
March R (1992) Visual reconstructions with discontinuities using variational methods. Image Vis Comput 10:30–38
Maute K, Kreissl S, Makhija D, Yang R (2011) Topology optimization of heat conduction in nano-composites. In 9th World congress on structural and multidisciplinary optimization. Shizuoka
Osher S, Fedkiw R (2003) Level set methods and dynamic implicit surfaces. Springer-Verlag, New York
Osher S, Santosa F (2001) Level set methods for optimization problems involving geometry and constraints: I. Frequencies of a two-density inhomogeneous drum. J Comput Phys 171(1):272–288
Osher S, Sethian JA (1988) Front propagating with curvature-dependent speed: algorithms based on Hamilton-Jacobi formulations. J Comput Phys 79:12–49
Pingen G, Waidmann M, Evgrafov A, Maute K (2010) A parametric level-set approach for topology optimization of flow domains. Struct Multidiscip Optim 41(1):117–131
Rozvany GIN, Zhou M, Birker T (1992) Generalized shape optimization without homogenization. Struct Multidiscip Optim 4(3–4):250–252
Sethian JA (1999a) Fast marching methods. SIAM Rev 41(2):199–235
Sethian JA (1999b) Level-set methods and fast marching methods: evolving interfaces in computational geometry, fluid mechanics, computer vision and materials science. Cambridge University Press, Cambridge
Sethian JA, Wiegmann A (2000) Structural boundary design via level set and immersed interface methods. J Comput Phys 163(2):489–528
Sokolowski J, Zochowski A (1999) On the topological derivatives in shape optimization. SIAM J Control Optim 37:1251–1272
Stolpe M, Svanberg K (2001) An alternative interpolation scheme for minimum compliance topology optimization. Struct Multidiscip Optim 22(2):116–124
Sussman M, Smereka P, Osher S (1994) A level set approach for computing solutions to incompressible two-phase flow. J Comput Phys 114:146–159
Suzuki K, Kikuchi N (1991) A homogenization method for shape and topology optimization. Comput Methods Appl Mech Eng 93(3):291–318
Svanberg K (1987) The method of moving asymptotoes - a new method for structural optimization. Int J Numer Methods Eng 24(2):359–373
Takezawa A, Nishiwaki S, Kitamura M (2010) Shape and topology optimization based on the phase field method and sensitivity analysis. J Comput Phys 229:2697–2718
Talischi C, Paulino GH, Pereira A, Menezes IFM (2010) Polygonal finite elements for topology optimization: a unifying paradigm. Int J Numer Methods Eng 82:671–698
Tsai R, Osher S (2003) Level set methods and their application in image science. Commun Math Sci 1:623–656
Van Dijk NP (2012) Pushing the boundaries: level-set mehods and geometrical nonlinearities in structural topology optimization. PhD thesis. Delft University of Technology
Van Dijk NP, Langelaar M, Van Keulen F (2009) A discrete formulation of a discrete level set method treating multiple contraints. 8th World congress on structural and multidisciplinary optimization. Lisbon
Van Dijk NP, Langelaar M, Van Keulen F (2012) Explicit level-set based topology optimization using an exact Heaviside function and consistent sensitivity analysis. Int J Numer Methods Eng 91(1):67–97
Van Dijk NP, Maute K, Langelaar M, Van Keulen F (2013) Level-set methods for structural topology optimization: a review. Struct Multidiscip Optim. doi:10.1007/s00158-013-0912-y
Wang MY (2005) Topology optimization with level set method incorporating topological derivatives. In 6th World congress on structural and multidisciplinary optimization, Rio de Janeiro
Wang MY, Wang XM (2004) Color level sets: a multi-phase method for structural topology optimization with multiple materials. Comput Methods Appl Mech Eng 193:469–496
Wang S, Wang MY (2006) Radial basis functions and level set method for structural topology optimization. Int J Numer Methods Eng 65:2060–2090
Wang MY, Zhou S (2004a) Phase field: a variational method for structural topology optimization. Comput Model Eng Sci 6(6):547–566
Wang MY, Zhou S (2004b) Synthesis of shape and topology of multi-material structures with a phase-field method. J Computer-Aided Mater Des 11:117–138
Wang MY, Wang X, Guo D (2003) A level-set method for structural topology optimization. Comput Methods Appl Mech Eng 192:227–246
Wang SY, Lim KM, Khoo BC, Wang MY (2007a) An extended level set method for shape and topology optimization. J Comput Phys 221(1):395–421
Wang SY, Lim KM, Khoo BC, Wang MY (2007b) On hole nucleation in topology optimization using the level set methods. Comput Model Eng Sci 21(3):219–237
Wei P, Wang MY (2006) Parametric structural shape and topology optimization method with radial basis functions and level-set mehod. In: Proceedings of international design engineering technical conferences & computer and information in engineering conference
Xia Q, Wang MY (2008) Topology optimization of thermoelastic structures using level set methods. Comput Mech 42(6):837–857
Yamada T, Izui K, Nishiwaki S, Takezawa A (2010) A topology optimization method based on the level set method incorporating a fictitious interface energy. Comput Methods Appl Mech Eng 199(45–48):2876–2891
Yamada T, Izui K, Nishiwaki S (2011) A level set-based topology optimization method for maximizing thermal diffusivity in problems including design-dependent effects. J Mech Des 133:031011–1–031011–9
Yamasaki S, Nishiwaki S, Yamada T, Izui K, Yoshimura M (2010) A structural optimization method based on the level set method using a new geometry-based re-initilization scheme. Int J Numer Methods Eng 83(12):1580–1624
Ye JC, Bresler Y, Moulin P (2002) A self-referencing level-set method for image reconstruction from sparse Fourier samples. Int J Comput Vis 50:253–270
Yoon GH, Kim YY (2005) Element connectivity parameterization for topology optimization of geometrically nonlinear structures. Int J Solids Struct 42(7):1983–2009
Yoon GH, Joung YS, Kim YY (2007) Optimal layout design of three-dimensional geometrically non-linear structures using the element

connectivity parameterization method. Int J Numer Methods Eng 69(6):1278–1304

Yoon GH, Kim YY, Langelaar M, Van Keulen F (2008) Theoretical aspects of the internal element connectivity parameterization approach for topology optimization. Int J Numer Methods Eng 76(6):775–797

Zhou S, Li Q (2008) A variational level set method for the topology optimization of steady-state Navier-Stokes flow. J Comput Phys 227(24):10178–10195

Zhuang CG, Xiong ZH, Ding H (2007) A level set method for topology optimization of heat conduction problem under multiple load cases. Comput Methods Appl Mech Eng 196(4–6):1074–1084